

Effect of Stellar Encounters on Comet Cloud Formation

A. Higuchi

Department of Earth and Planetary Sciences, Faculty of Science, Tokyo Institute of
Technology, Meguro, Tokyo 152-8551

and

E. Kokubo

Division of Theoretical Astronomy, National Astronomical Observatory of Japan, Mitaka,
Tokyo 181-8588

Received _____; accepted _____

ABSTRACT

We have investigated the effect of stellar encounters on the formation and disruption of the Oort cloud using the classical impulse approximation. We calculate the evolution of a planetesimal disk into a spherical Oort cloud due to the perturbation from passing stars for 10 Gyr. We obtain the empirical fits of the e -folding time for the number of Oort cloud comets using the standard exponential and Kohlrausch formulae as functions of the stellar parameters and the initial semimajor axes of planetesimals. The e -folding time and the evolution timescales of the orbital elements are also analytically derived. In some calculations, the effect of the Galactic tide is additionally considered. We also show the radial variations of the e -folding times to the Oort cloud. From these timescales, we show that if the initial planetesimal disk has the semimajor axes distribution $dn/da \propto a^{-2}$, which is produced by planetary scattering (Higuchi et al. 2006), the e -folding time for planetesimals in the Oort cloud is ~ 10 Gyr at any heliocentric distance r . This uniform e -folding time over the Oort cloud means that the supply of comets from the inner Oort cloud to the outer Oort cloud is sufficiently effective to keep the comet distribution as $dn/dr \propto r^{-2}$. We also show that the final distribution of the semimajor axes in the Oort cloud is approximately proportional to a^{-2} for any initial distribution.

Subject headings: Oort Cloud — comets: general

1. INTRODUCTION

The Oort Cloud is a spherical comet reservoir surrounding the Solar system (Oort 1950). Observations and statistical studies estimate that it consists of more than 10^{12} comets and is on the order of 10^4 - 10^5 AU in size (e.g., Dones et al. 2004). This structure can be described as an assembly of comets whose perihelion distances extend outside the planetary region, aphelion distances smaller than the tidal radius of the Sun (~ 1 pc), and a nearly isotropic inclination distribution. Now it is generally accepted that the comets are residual planetesimals from planet formation and are originally inside the planetary region.

In the standard scenario of the Oort cloud formation, these residual planetesimals with small eccentricities and inclinations are scattered by giant planets and their semimajor axes and eccentricities are raised. Such planetesimals with large aphelion distances are affected by external forces. The perihelion distances are pulled out of the planetary region and the inclinations are randomized by external forces and then the spherical structure of the Oort cloud is attained. The perturbation from passing stars is the only external force considered in the original Oort scenario. Many authors have studied the effect of the external forces and now we recognize that not only passing stars, but also the Galactic disk and giant molecular clouds are effective perturbers (e.g., Dones et al. 2004).

Among these external forces, the most effective one is the Galactic tide (e.g., Harrington 1985; Byl 1986; Heisler & Tremaine 1986). The Galactic tide can efficiently raise the perihelion distances of planetesimals with large semimajor axes and eccentricities. Higuchi et al. (2007) derived the analytical formulae for time evolution of orbital elements of planetesimals under the effect of the Galactic tide. They considered the vertical component of the Galactic tide against the Galactic plane, which is ~ 10 times larger than the other components. They showed that the inclination distribution attained by the Galactic tide in 5 Gyr is far from the isotropic one, which is expected from the observations of long-period

comets. This is because the Galactic tide causes, not the randomization, but the periodic oscillations of orbital elements and the synchronized evolution of the orbital elements produces two peaks in the inclination distribution. Also, the inclination range attained by the vertical component of the Galactic tide is not from 0 to 180° , but the function of the inclination of the ecliptic plane against the Galactic plane. In the case of the Solar system, a planetesimal initially on the ecliptic plane cannot attain an inclination larger than 153° .

Passing stars randomize and eject planetesimals from the Solar system by giving velocity kicks, while the vertical component of the Galactic tidal force does not change the energy of the planetesimals. The perturbations from passing stars, due to their random-walk nature, may play an important role in the production of the nearly isotropic inclination distribution of planetesimals. Many authors have examined this effect, mainly by analytical approach (e.g., Heisler et al. 1987; Dybczyński 2002; Fouchard et al. 2011). Their main interest is in the production of long-period comets from the spherical Oort cloud.

The direct simulation of the Oort cloud formation including the perturbations from giant planets, the Galactic disk, and passing stars was first done by Duncan et al. (1987) and redone by Dones et al. (2004) with more realistic initial conditions. Dones et al. (2004) showed the time evolution of the mean eccentricity and inclination of planetesimals and their dependencies on the initial semimajor axes. In their calculation, the mean values expected for the isotropic distribution of planetesimals are attained in 4.5 Gyr, for the semimajor axis larger than 10^4 - 2×10^4 AU. However, the time evolution of the distributions of the eccentricities and inclinations, and the role of stellar encounters in their evolution are not clarified.

In the present paper we investigate the effect of stellar encounters on the evolution of a planetesimal disk, from the point of view of Oort Cloud formation. We obtain (i) the impact parameters that describe the evolution timescales of the orbital elements. (ii) the decay

timescales (e -folding time) of surviving comets in the solar system, and its radial variations, and (iii) the evolution of the semimajor axis distribution in the Oort cloud. We use the classical impulse approximation (e.g., Rickman 1976; Rickman et al. 2005) to calculate the velocity change of planetesimals induced by stellar encounters. The outline of this paper is as follows: We first describe the basic dynamics of planetesimals due to a stellar encounter in Section 2. In Section 3, we describe the numerical model of our simulations. The results are presented in Section 4. Section 5 is devoted to a summary and discussion.

2. BASIC DYNAMICS

We use the classical impulse approximation to calculate the velocity change given by a stellar encounter (Rickman 1976). In this approximation, a planetesimal is held fixed with respect to the Sun, a star passes with constant velocity along the straight line, and the time intervals before and after the closest approach are assumed to be infinity. Then, the velocity change of the planetesimal is given by

$$\Delta \mathbf{v} = \frac{2Gm_*}{v_*} \left(\frac{\mathbf{b}_p}{b_p^2} - \frac{\mathbf{b}}{b^2} \right), \quad (1)$$

where G is the gravitational constant, m_* and v_* are the stellar mass and velocity, and \mathbf{b}_p and \mathbf{b} are the position vectors to the star from the planetesimal and the Sun, respectively.

In this section, we derive the impact parameters that can be the indexes for the orbital evolution. We deal only with planetesimals that have the orbital velocity much lower than the typical passing star, i.e., the planetesimals with $a \gtrsim 10^3$ AU.

2.1. Ejection

Assuming $\mathbf{b}_p \ll \mathbf{b}$, we use the following simplified equation instead of Equation (1),

$$\Delta v \simeq \frac{2Gm_*}{v_*} \frac{1}{b_p}. \quad (2)$$

Substituting $\Delta v = v_{\text{esc}} = \sqrt{2GM_\odot/r}$ into Equation (2), we obtain the impact parameter of the star-planetesimal encounter that gives the velocity change large enough to escape from the Solar system,

$$b_{\text{esc}} = \frac{m_*}{v_*} \sqrt{\frac{2G}{M_\odot}} r, \quad (3)$$

where r is the heliocentric distance of the planetesimal and we used $v \ll \Delta v$. This condition is basically satisfied when a planetesimal is near its aphelia. When $\mathbf{b}_p \gg \mathbf{b}$, b_p in Equation

(2) is substituted by b . Then we obtain the impact parameter of the star-Sun encounter that gives the velocity change large enough to escape from the Solar system to the planetesimal with r , which is identical to Equation (3). This is the same to the other impact parameters derived in Sections 2.2 and 2.3.

Using b_{esc} , we derive the parameter dependence of the survival rate of planetesimals in the Solar system P_{bound} analytically by improving Weissman’s method (Weissman 1980). Weissman (1980) estimated the fraction of the Oort cloud comets ejected by a single stellar encounter by assuming that a star drills a narrow tunnel through the Oort cloud, ejecting all the planetesimals within a radius of b_{esc} . Assuming a constant number density of planetesimals in the Oort cloud and the length of the tunnel equal to the mean chord length, Weissman (1980) estimated that nine percent of the cloud population is ejected by a single encounter with a $1 M_{\odot}$ star with relative velocity 20 km s^{-1} . Using the same assumption, we express the ratio of the number of planetesimals ejected by a stellar encounter to that of surviving planetesimals as

$$A \simeq \frac{2\pi b_{\text{esc}}^2}{\pi R_c^2} \propto a^{-1} \left(\frac{m_*}{v_*} \right)^2, \quad (4)$$

where a is the semimajor axis and we used $r \propto R_c \propto a$. The factor 2 of πb_{esc}^2 expresses the contributions from stellar encounters with planetesimals and the Sun. Additionally assuming that R_c is constant with time, the number of stellar encounters within $b < R_c$ in time t is proportional to

$$B \propto f_{\text{enc}} R_c^2 t \propto a^2 t, \quad (5)$$

where f_{enc} is the encounter frequency per 1 Myr within 1 pc from the Sun. Using A and B , P_{bound} is expressed as an exponential decay,

$$P_{\text{bound}} = (1 - A)^B \simeq \exp \left(-\frac{t}{t_e} \right), \quad (6)$$

where we used $A \ll 1$, and t_e is the e -folding time of the Oort cloud,

$$t_e \propto a^{-1} \left(\frac{m_*}{v_*} \right)^{-2} f_{\text{enc}}^{-1}. \quad (7)$$

2.2. Eccentricity change

Next, we define the star-planetesimal impact parameter b_e , for which a planetesimal gains the eccentricity change Δe . We consider a planetesimal in the Cartesian coordinates (x, y, z) centered on the Sun and the x -axis is chosen as parallel to the position vector of the planetesimal from the Sun. The x - y plane agrees with its orbital plane (hereafter referred to as the reference plane). Then the position is written as $\mathbf{r} = (r, 0, 0)$.

$$\mathbf{e} = \frac{v^2 \mathbf{r} - (\mathbf{v} \cdot \mathbf{r}) \mathbf{v}}{GM_\odot} - \frac{\mathbf{r}}{r}. \quad (8)$$

After a stellar encounter that gives the planetesimal the velocity change of $\Delta \mathbf{v} = (\Delta v_x, \Delta v_y, \Delta v_z)$, the planetesimal has the new eccentricity vector \mathbf{e}' . The velocity change due to a stellar encounter is given by

$$\Delta \mathbf{v} = \begin{pmatrix} \Delta v_x \\ \Delta v_y \\ \Delta v_z \end{pmatrix} = \Delta v \begin{pmatrix} \cos \alpha \\ \sin \alpha \cos \beta \\ \sin \alpha \sin \beta \end{pmatrix} \quad (9)$$

where $\cos \alpha$ and β are randomly chosen from a uniform distribution between -1 and 1 and 0 and 360° , respectively, since stellar encounters occur with random direction with respect to the Sun and the planetesimal. The change of the eccentricity vector is expressed as

$$\Delta \mathbf{e} = \mathbf{e}' - \mathbf{e} = \frac{r}{GM_\odot} \begin{pmatrix} (\Delta v)^2 - (\Delta v_x)^2 \\ -\Delta v_x \Delta v_y \\ -\Delta v_x \Delta v_z \end{pmatrix}, \quad (10)$$

where we used the approximation $\mathbf{v} \ll \Delta \mathbf{v}$. Then the absolute value of the eccentricity vector change is given as

$$\Delta e = \frac{r \Delta v}{GM_\odot} [(\Delta v)^2 - (\Delta v_x)^2]^{1/2} = \frac{r(\Delta v)^2}{GM_\odot} \sin \alpha. \quad (11)$$

From Equation (11), we obtain the velocity change required for the change of Δe

$$\Delta v_{\Delta e} = \sqrt{\frac{GM_\odot}{r} \frac{\Delta e}{\sin \alpha}}. \quad (12)$$

Combining Equations (2) and (12), we have

$$b_e = 2 \frac{m_*}{v_*} \sqrt{\frac{G}{M_\odot} \frac{r}{\Delta e} \sin \alpha} \simeq \sqrt{\frac{2 \sin \alpha}{\Delta e}} b_{\text{esc}}. \quad (13)$$

The ratio between the cross-sections derived from Equations (3) and (13) is ~ 2 for $\sin \alpha \simeq \Delta e$. This ratio implies that when one planetesimal escapes from the solar system due to a stellar encounter, another planetesimal reduces its eccentricity and evolves into a nearly circular orbit. Additionally, Equation (13) tells us that Δe is Lévy flight: the probability for a planetesimal having $\Delta e > \epsilon$ by a single stellar encounter $P(\Delta e > \epsilon)$, which is expected to be proportional to b_e^2 , follows $P(\Delta e > \epsilon) \propto \epsilon^{-1}$ (e.g., Mandelbrot 1982). The other examples of the Lévy flight are found in the semimajor axis evolution of planetesimals by planetary scattering (see Appendix. A) and in the evolution of the eccentricity and inclination of the binary interacting with unbound perturbers (Collins & Sari 2008).

Next, we define the change of the argument of perihelion $\Delta \omega$ as

$$\cos \Delta \omega \equiv \frac{\mathbf{e} \cdot \mathbf{e}'}{|\mathbf{e}| |\mathbf{e}'|}. \quad (14)$$

Under the assumptions of $\mathbf{v} \cdot \mathbf{r} = 0$ and $v \ll \Delta v$, we have $\mathbf{e} \simeq (-1, 0, 0)$ and then $|\mathbf{e}| \simeq 1$.

Substituting $\mathbf{v}' = \mathbf{v} + \Delta \mathbf{v}$ into Equation (8), we obtain

$$\mathbf{e}' \simeq \begin{pmatrix} \frac{(\Delta v)^2 r}{GM_\odot} \sin^2 \alpha - 1 \\ -\frac{(\Delta v)^2 r}{GM_\odot} \cos \alpha \sin \alpha \cos \beta \\ -\frac{(\Delta v)^2 r}{GM_\odot} \cos \alpha \sin \alpha \sin \beta \end{pmatrix}. \quad (15)$$

When $\Delta\omega = 90^\circ$,

$$\mathbf{e} \cdot \mathbf{e}' = 1 - \frac{(\Delta v)^2 r}{GM_\odot} \sin^2 \alpha = 0 \quad (16)$$

Substituting Equation (2) into Equation (16), we obtain the impact parameter b_ω that gives the planetesimal $\Delta\omega = 90^\circ$,

$$b_\omega = 2 \frac{m_*}{v_*} \sqrt{\frac{G}{M_\odot}} r \sin \alpha = \sqrt{2} \sin \alpha b_{\text{esc}}. \quad (17)$$

Equation (17) tells us that b_ω is on the same order of b_e for $\Delta e = 1$ but slightly smaller than it since $\sin \alpha \leq 1$ and the mean value of $\sin \alpha$ is $\pi/4 < 1$.

2.3. Inclination change

We define Δi as an inclination of the planetesimal against the reference plane after a stellar encounter. Under the same assumption used in the derivation of b_e , the angular momentum of the planetesimal after a stellar encounter is written as

$$\mathbf{h}' = \mathbf{r} \times (\mathbf{v} + \Delta \mathbf{v}) = \begin{pmatrix} 0 \\ -r\Delta v_z \\ r(v + \Delta v_y) \end{pmatrix} = h' \begin{pmatrix} \sin \Delta\Omega \sin \Delta i \\ \cos \Delta\Omega \sin \Delta i \\ \cos \Delta i \end{pmatrix} \quad (18)$$

where $\Delta\Omega$ is the longitude of the ascending node from the x -axis. Under the impulse approximation, h'_x , the x -component of \mathbf{h}' , is always 0 because the x -axis lies on the orbital plane of the planetesimal. Using $h'_x = h' \sin \Delta\Omega \sin \Delta i = 0$ in Equation (18), we have $\Delta\Omega = 0$, which means Ω is not changed by a velocity kick given at the aphelion. Thus, Δi can be written as

$$\Delta i = \arctan \left(\frac{h'_y}{h'_z} \right) = \arctan \left(\frac{\Delta v_z}{v + \Delta v_y} \right). \quad (19)$$

Assuming $\Delta v \gg v$ in Equation (19), and using Equation (9), we have

$$\Delta i = \begin{cases} \beta & (\beta < 180^\circ) \\ \beta - 180^\circ & (\beta > 180^\circ) \end{cases},$$

where β is uniformly distributed between 0 and 360° .

Here we use $\Delta v = v$ as a condition to derive the impact parameter b_i , which gives the planetesimal $\Delta i = 90^\circ$. The orbital velocity of the planetesimal at its aphelion v_Q is written as

$$v_Q = \sqrt{\frac{2GM_\odot(1-e)}{Q}}, \quad (20)$$

where Q is the aphelion distance. Using $\Delta v = v_Q$ and $r = Q$ in Equation (2), we obtain

$$b_i = 2\frac{m_*}{v_*} \sqrt{\frac{G}{M_\odot} \frac{r}{(1-e)}} = \sqrt{\frac{2}{(1-e)}} b_{\text{esc}}, \quad (21)$$

which means that for $1-e \simeq 10^{-3}$, when one planetesimal escapes from the solar system due to a stellar encounter, other ~ 2000 planetesimals gain $\sim 90^\circ$ inclinations. Comparing b_i to b_e or b_ω , we find that the timescale the i -distribution requires to relax is about three orders of magnitude shorter than that for the e -distribution.

3. METHOD OF CALCULATION

We describe the initial distribution of planetesimals and stellar parameters, and the orbital evolution of planetesimals by stellar encounters. The parameter sets of all models are summarized in Tables 1, 2, and 3.

3.1. Planetesimal Disks

We set up initial planetesimal disks formed by the transportation of planetesimals due to planetary scattering. In such planetesimal disks, planetesimals have their perihelion distances in the planetary region with small inclinations. We performed the test calculations and found that the disk evolution depends mainly on the semimajor axis, and weakly on the

perihelion distance if it is inside the planetary region and $a \gtrsim 10^3$ AU (i.e., $e \sim 1$). Thus, for simplicity, we consider planetesimals with perihelion distances $q_0 = 10$ AU and inclinations $i_0 = 0$ as the standard (I0) model (hereafter we use the subscript 0 for the initial value). The initial semimajor axes of the planetesimals are $a_0 = 5 \times 10^3, 10^4, 1.5 \times 10^4, \dots$, and 5×10^4 AU. Their initial angle variables, the argument of perihelion ω_0 , the longitude of ascending node Ω_0 , and the mean anomaly M_0 are uniformly distributed in the range 0 - 360° . Additionally, we prepare spherical Oort clouds that have uniform distributions of $-1 < \cos i < 1$ and $10 \text{ AU} < q < a_0$ as initial conditions to evaluate the effect of the cloud shape on the decay time scale (I2 in Table 1). Each disk or cloud consists of 10^4 planetesimals with identical a_0 .

To investigate the radial variation of the structure and evolution of the whole disk, we consider planetesimal disks that have broad a_0 -distributions in $5 \times 10^3 \text{ AU} < a_0 < 5 \times 10^4 \text{ AU}$ as summarized in Table 2. The a_0 -distribution for the standard model (W0) follows $dn/da_0 \propto a_0^\gamma$, where $\gamma = -2$ (Higuchi et al. 2006), which is a flat distribution in $E = 1/a$ (see Appendix). We test four additional disks for $\gamma = 0, 1, -3$, and -1 for comparison (W1, W2, W4, and W5). Each disk consists of 5×10^5 planetesimals.

3.2. Passing Stars

The stellar encounters are assumed to occur with random directions and follow the distribution $dn_s/db \propto b$, where n_s is a number of stellar encounters. The time interval to the next stellar encounter is given according to a Poisson distribution (Heisler et al. 1987). The star sets are described by five parameters; the stellar mass m_* and velocity v_* , the encounter frequency f_{enc} (in number per 1 Myr within 1 pc from the Sun), and the minimum and maximum impact parameters b_{min} and b_{max} .

We consider two types of star sets. First, we generate the star sets that consist of stars with identical m_* chosen between $0.25M_\odot$ and $2M_\odot$, and $v_* = 20 \text{ kms}^{-1}$ (under the impulse approximation, the important value is m_*/v_* and we can fix one of m_* or v_*). We choose $m_* = 0.5M_\odot$ as the standard model. The second star sets consist of stars with the realistic distributions of m_* and v_* with f_{enc} for each type of star, based on the observations of the Solar neighborhood (I3 in Table 1 and W4 in Table 2).

The stellar mass used in the standard model $m_* = 0.5M_\odot$ is estimated from the observations. Let us assume that the energy change due to a kick by k -type star can be written as

$$\Delta E_k \propto (\Delta v)^2 \propto \left[\frac{m_{*,k}}{v_{*,k}} g(b, b_p) \right]^2, \quad (22)$$

where we assume $g(b, b_p)$, the term given as a function of the impact parameters, is independent of k . The stellar velocity $v_{*,k}$ is given as

$$v_{*,k}^2 = v_\odot^2 + 3\sigma^2 - 2\sqrt{3}v_\odot\sigma \cos \theta, \quad (23)$$

where v_\odot is the solar apex velocity, σ is the 1D velocity dispersion, and θ is a direction angle between v_* and σ that has a uniform distribution between 0 and 360° . We assume that the typical parameters \bar{f}_{enc} , \bar{m}_* , and \bar{v}_* satisfy the following equation, which is derived by averaging over θ and summing up the energy changes from all types of stars,

$$\sum_{k=0}^{13} f_{\text{enc},k} m_{*,k}^2 \langle v_{*,k}^{-2} \rangle = \bar{f}_{\text{enc}} \left(\frac{\bar{m}_*}{\bar{v}_*} \right)^2. \quad (24)$$

Adopting v_\odot , σ , f_{enc} and m_* in Table 3, $\bar{f}_{\text{enc}} = 10$ and $\bar{v}_* = 20 \text{ kms}^{-1}$, we have $\bar{m}_* \simeq 0.5M_\odot$.

To generate the distributions of m_* and v_* , we follow the procedure described in Rickman et al. (2008) and use the same values of v_\odot and σ , which are taken from Table 8 of Garcia-Sanchez et al. (2001) and Allen (1985). This realistic star set consists of 13 types of stars. The star data in this paper is summarized in Table 3. The sum of the

encounter frequency of all types of stars is estimated to be $f_{\text{total}} \simeq 10.5$ (e.g., Heisler et al. 1987; Rickman et al. 2004, 2008). Then one can estimate that one star approaches the Sun within 0.005 pc ($\sim 10^3$ AU) in 5 Gyr. Although we calculate the evolution for 10 Gyr, we set $b_{\text{min}} = 0.005$ pc for all star sets and $b_{\text{max}} = 1$ pc for the standard model (I0). It has been said that the effect of the stars for $b \gtrsim 1$ pc is smaller than that of stars with $b \leq 1$ pc (e.g., Weissman 1980). We also perform several calculations to evaluate the effect of distant stars with $b_{\text{max}} = 0.25, 0.5$ and 2 pc (models I4, I5, and I6) and find that the differences among $b_{\text{max}} = 0.25, 0.5, 1$, and 2 pc are small if $2a_0 < b_{\text{max}}$. Therefore, $b_{\text{max}} = 1$ pc is appropriate for the Oort cloud with $R_c = 10^5$ AU. We can also show it analytically (see Appendix).

We perform 10 runs for each model with different orientations and time of stellar passages that are randomly chosen. The error bars shown in the following figures indicate the 1- σ error from the 10 runs.

3.3. Orbital Evolution

We describe the procedures to calculate the orbital evolution due to stellar encounters and the Galactic tide. We develop a hybrid code that takes into account both stellar perturbations and the Galactic tide.

3.3.1. Stellar encounters

To calculate the orbital change of planetesimals due to the perturbation from a passing star, we use the classical impulse approximation that gives the velocity change described in Equation (1). For the impulse approximation to give a reasonable result, the Kepler period of the planetesimal must be longer than the typical encounter time of a star with the Sun ($\sim 10^5$ yr). We choose the minimum value of $a_0 = 5 \times 10^3$ AU from this restriction.

Rickman et al. (2005) showed that the classical impulse approximation gives a reasonably good approximation for the Oort cloud simulation as long as we avoid too close and/or too slow encounters.

We calculate the orbital evolution of planetesimals by adding the velocity change for 10 Gyr. If a planetesimal has its heliocentric distance $r > 1$ pc, it is counted as an escaper from the Solar system and discarded from the calculation. This criterion is not equivalent to $e > 1$, but we found that with some extra calculations that it is almost the same. The calculation is stopped when the survival rate $P_{\text{bound}} \equiv n/n_0 < 10^{-3}$ or at 10 Gyr.

3.3.2. Galactic tide

We add the effect of the vertical component of the Galactic tidal force to the standard model (I1 in Table 1 and W3 in Table 2). This effect is analytically computed using the formulae derived in Higuchi et al. (2007). Higuchi et al. (2007) investigated the effect of the Galactic tide on the orbits of Oort cloud comets and obtained the evolution of the e , i , ω , and Ω in the Galactic coordinates (note a does not change since the energy is conserved). They neglected the radial component of the Galactic tide so the energy and z -component of the angular momentum of comets are conservative quantities. The period of the oscillations of e , i , and ω and the mean period of the circulation of Ω are as follows:

$$t_{e,i,\omega} = \frac{\pi}{n_{\omega^*}}, \quad (25)$$

$$t_{\Omega^*} = \frac{\pi^2}{A_3 \Pi[K(k), \alpha^2, k] n_{\omega^*}}, \quad (26)$$

where n_{ω^*} is a mean motion of ω^* that is an angle variable directly related to ω , A_3 , α , and k are constants given by initial orbital elements of each planetesimal, Π is an elliptic integral of the third kind, and $K(k)$ is a complete elliptic integral of the first kind. The derivation of the timescales and constants are given in Higuchi et al. (2007). Note that in

Higuchi et al. (2007) $T_{e,i,\omega}$ is written as P_{ω^*} , the factor of Equation (A24) is not correct ¹, and t_{Ω^*} , which is written as P_{Ω^*} , is given in a different form using a Fourier series. We assume that the timescale of the evolution due to the Galactic tide is $\propto P_{e,i,\omega}$ or P_{Ω} . Both $P_{e,i,\omega}$ and P_{Ω} are proportional to $n_{\omega^*}^{-1}$, which is

$$n_{\omega^*} = \frac{\nu_0^2}{n'} \frac{\pi}{2K(k)} \sqrt{\alpha_2 - \alpha_0} \propto a^{3/2}, \quad (28)$$

where ν_0 is a vertical frequency of the solar motion in the Galactic disk that is constant, n' is the mean motion and α_0 and α_2 are the constants given by the initial orbital elements of the planetesimal. Then the timescale is proportional to $a^{-3/2}$. The evolution timescales of these orbital elements except Ω are coupled. That means the Galactic tide itself does not randomize the planetesimal distribution. Though the evolution of Ω is independent of those of the other orbital elements, their periods are nearly commensurable. Therefore, at the beginning of the evolution, i and Ω are nearly coupled and make two strong peaks in the inclination distribution around 27° and 153° with respect to the ecliptic plane, where the inclination of the ecliptic plane to the Galactic disk is assumed to be 63° .

In the simulations, planetesimals are affected by the Galactic tide during the time intervals between one stellar encounter and the next. After each stellar encounter, the new conservative quantities of planetesimals are recalculated. We adopt the total density in the solar neighborhood $\rho = 0.1 M_{\odot} \text{pc}^{-3}$ (Holmberg & Flynn 2000).

¹ The factor A_2 in Equation (A24) in Higuchi et al. (2007) should be A_3 ,

$$A_3 = \frac{2}{A_1 \sqrt{\alpha_2 - \alpha_0}} A_2 = \frac{j x_0^* - j^2}{2 \alpha_0 - j^2} \frac{1}{\sqrt{\alpha_2 - \alpha_0}}. \quad (27)$$

4. RESULTS

4.1. Planetesimal Disks with Identical a_0

We present the results of simulations for initial planetesimal disks that consist of planetesimals with identical a_0 . First, we show the result for the standard model with $a_0 = 2 \times 10^4$ AU. Next, we compare the results for different a_0 and those with the Galactic tidal force.

4.1.1. Evolution of Distributions

Figure 1 shows snapshots of the planetesimal disk plotted on the x - z plane of the Cartesian coordinates (x, y, z) for $t = 1$ Myr, 5 Myr, 10 Myr, ..., and 10 Gyr. The planetesimal disk is initially on the $z = 0$ plane. The planetesimals initially have $a_0 = 2 \times 10^4$ AU. By 10 Myr, the disk is almost flat. Some asymmetric structures seen at 5 Myr and 10 Myr are the result of recent stellar encounters. At 100 Myr, the disk slightly expands from the initial size and has thickness of $\sim 10^4$ AU. The planetesimal distribution expands to around 10^5 AU and becomes almost spherically symmetric at 5 Gyr and shrinks by 10 Gyr.

For quantitative analysis of the structure evolution, we introduce an indicator R_p that is the heliocentric distance that contains p percent of surviving planetesimals inside it. The time evolution of R_{90} scaled by a_0 (i.e., $R_{100} \simeq 2a_0$ at $t = 0$) is plotted in Figure 2. The structure becomes the largest in R_{90} at $\simeq 2$ Gyr for $a_0 = 2 \times 10^4$ AU. After reaching the maximum, it shrinks. The time evolution of R_{90} for the other parameters is also plotted in Figure 2. The evolution of R_{90} for $m_* = 1M_\odot$ is quantitatively the same as that for $m_* = 0.5M_\odot$, but it is much more rapid, reaching the maximum value at $\simeq 1$ Gyr. The evolution for $m_* = 0.25M_\odot$ is slow and does not show the decrease in R_{90} within 10 Gyr. The dependence of the maximum R_{90} on a_0 is not well scaled by a_0 . The larger a_0 has the

shorter evolution timescale and smaller maximum value of R_{90}/a_0 . This is simply because the maximum heliocentric distance for bound planetesimals is $r_{\text{esc}} = 1$ pc in our model, which is independent of a_0 .

Figures 3-6 show the time evolution of distributions of semimajor axes, eccentricities, inclinations, and arguments of perihelion of the planetesimals plotted in Figure 1, respectively. In 5 Gyr, the semimajor axis distribution evolves approximately into $dn/da \propto a^{-2}$. The diffusion is not symmetric about the initial value. At the beginning of the evolution, there are more planetesimals for $a > a_0$. The mean value of a shifts and it reaches $\sim 4 \times 10^4$ AU. After the outward shift, the a -distribution finally shifts inward and the mean value of a decreases to $\sim 3 \times 10^4$ AU at 10 Gyr, since planetesimals with larger a are easily removed from the disk.

The short-dash curve plotted in the e - and i -distributions is the distribution expected for an isotropic distribution. The eccentricity distribution in Figure 4 gradually relaxes and attains the isotropic distribution, which is proportional to e . On the other hand, the inclination distribution shown in Figure 5 relaxes much more rapidly compared to those of the other orbital elements. Only in 5 Myr, the distribution already has its range from 0 to 180° . This rapid spread of i -distribution compared to the other orbital elements and the flat distribution are explained in Equation (20) in section 2.3. They are at the stage where only the i -distribution has relaxed its initial distribution, but the other orbital element distributions have not yet. The i -distribution ranging from 0 to 180° does not mean the Oort cloud is spherical. To be a spherical Oort cloud, the isotropic distribution of ω is also required. Figure 6 shows the time evolution of the ω -distribution. In 5 Myr, the ω -distribution is concentrated at $\omega = 0$ (or $\omega = 180^\circ$ if $i > 90^\circ$) i.e., the eccentricity vectors are still close to the initial plane.

Figure 7 compares the evolution of i -distribution due to the passing stars only (I0,

left), the Galactic tide only (GT, center), and both of them (I1, right) for $a_0 = 2 \times 10^4$ AU at 50 Myr, 500 Myr, and 5 Gyr. Two peaks in the i -distribution seen in GT (center) are the strong feature made by the Galactic tide. They are also seen in 500 Myr of the I1 model. The distribution for I1 is just intermediate between those with and without the Galactic tide. At 5 Gyr, the difference between the distributions with and without the Galactic tide is quite small. The random-walk nature of passing stars can randomize the angular momenta of planetesimals quickly, with much shorter timescale than that for ejection, as shown in section 2.3.

4.1.2. Decay of Comet Clouds

As described in the previous section, the number of planetesimals decreases while the e - and i -distributions approach the isotropic distribution. We fit the decay curve empirically using the standard exponential decay curve and the stretched exponential decay defined by the Kohlrausch formula (Dobrovolskis et al. 2007).

The empirical fit for P_{bound} obtained by the least-square fit optimized for $a_0 = 2 \times 10^4$ AU is

$$P_{\text{bound}}^{\text{fit}} = \exp\left(-\frac{t}{t_e^{\text{fit}}}\right), \quad (29)$$

$$t_e^{\text{fit}} \simeq 5.6 \left(\frac{a_0}{2 \times 10^4 \text{ AU}}\right)^{-1.4} \left(\frac{m_*}{0.5 M_\odot} \frac{20 \text{ kms}^{-1}}{v_*}\right)^{-1.7} \left(\frac{f_{\text{enc}}}{10 \text{ Myr}^{-1}}\right)^{-1} \text{ Gyr}. \quad (30)$$

We compare Equation (30) to a previous study on the lifetime of wide binaries. Weinberg et al. (1987) analytically and numerically calculated the lifetime of a binary as a function of the original binary semimajor axis (a_0) and other parameters of the perturbers. Weinberg et al. (1987) showed the characteristic lifetime of a binary with relatively small initial semimajor axis ($\lesssim 0.1$ pc) is proportional to a_0^{-1} . Tremaine (1993) referred to this to

describe the lifetime of the Oort cloud. Weinberg et al. (1987) also show that the lifetime is proportional to $n_*^{-1} M_*^{-2} V_{\text{rel}}$, where n_* is the number density of perturbers ($\propto f_{\text{enc}}/v_*$), M_* is the mass of a perturber, and V_{rel} is the relative velocity between the binary and the perturber. The dependence on a_0 in Equation (30) is close to -1.34, which is for a wide binary with the separation $\gtrsim 0.1$ pc shown in Weinberg et al. (1987).

The curves in Figure 8 are Equation (29) using Equation (30) for each parameter set. They agree well with P_{bound} . The differences between Equations (7) and (30) are basically due to the two assumptions for Equation (7) : (1) R_c is constant over the evolution, and (2) $\Delta v \gg v$ in derivation of b_{esc} . The reason the dependence on a_0 in Equation (30) is stronger than that in Equation (7) may be due to the evolution of a . The assumption of the constant $R_c(\propto a_0)$ is obviously broken, as seen in the evolution of R_{90} in Figure 2. As a evolves, the evolution of the Oort cloud is accelerated and the dependence on a_0 becomes stronger.

The stretched exponential decay is given by the Kohlrausch formula,

$$P_{\text{bound}} = \exp \left(- \left(\frac{t}{t_0} \right)^\beta \right), \quad (31)$$

where t_0 is a constant and β is the index known as the stretching parameter (Dobrovolskis et al. 2007). When $\beta = 1$, Equation (31) is the standard exponential decay and $t_0 = t_e$. The e -folding time is given as

$$t_e \equiv \frac{P_{\text{bound}}}{|dP_{\text{bound}}/dt|} = \beta^{-1} t_0^\beta t^{1-\beta}, \quad (32)$$

which indicates that t_e decreases and increases with time for $\beta > 1$ and $\beta < 1$, respectively.

We calculate t_0 and β using the least-square fit and obtain

$$t_0^{\text{fit}} = 5.3 \left(\frac{a_0}{2 \times 10^4 \text{ AU}} \right)^{-1.4} \left(\frac{m_*}{0.5 M_\odot} \frac{20 \text{ kms}^{-1}}{v_*} \right)^{-1.7} \left(\frac{f_{\text{enc}}}{10 \text{ Myr}^{-1}} \right)^{-0.97} \text{ Gyr}, \quad (33)$$

and

$$\beta^{\text{fit}} = 2.0 P_{\text{bound}}^{0.4}, \quad (34)$$

which shows that Equation (31) is now an implicit function of P_{bound} . As seen in Equation (34), β is not a constant over the evolution. Initially β is much larger than 1 and decreases with P_{bound} and when $P_{\text{bound}} \simeq 0.18$, $\beta \simeq 1$. The fits expressed by Equations (33) and (34) agree much better than those with the standard exponential decay, Equation (30).

All the analytical arguments in Section 2 are done under the assumption that the Oort cloud is spherical, despite the initial flat distributions of planetesimals. To see how it affects the results, we also perform the same calculations for the initially spherical cloud (I2 in Table 1). The e -folding time of the I2 model is plotted against a_0 in Figure 9. We found that the e -folding times of the I2 and I0 models are almost indistinguishable and the effect of the initial flat structure is negligible in P_{bound} under the random and many stellar encounters.

Figure 10 shows P_{bound} for the realistic star sets (I3) against time with $P_{\text{bound}}^{\text{fit}}$ for $f_{\text{enc}} = 10$, $v_* = 20 \text{ km s}^{-1}$, and $m_* = 0.5 M_{\odot}$. The error bars are large due to stochastic close encounters of massive stars, mostly B0 stars. However, the estimation of the evolution due to the realistic stars using $P_{\text{bound}}^{\text{fit}}$ for $f = \bar{f}_{\text{enc}}$, $v_* = \bar{v}_*$, and $m_* = \bar{m}_*$ agrees with P_{bound} within $1\text{-}\sigma$. Figure 11 shows the time t_e against a_0 with $1\text{-}\sigma$ error bars and t_e^{fit} for $m_* = 0.5 M_{\odot}$. They also agree within $1\text{-}\sigma$ except for $a_0 = 10^4 \text{ AU}$. This agreement between I0 and I3 shows that the averaging of energy kicks from many types of stars described in Section 3.2 is a good approximation.

The Galactic tide makes little difference in t_e as seen in Figure 9. It is easy to understand, because the Galactic tide in our model does not change the energy of planetesimals or the cross-section of the Oort cloud ($\sim a_0$). The timescale of the evolution due to the Galactic tide is proportional to $a_0^{-3/2}$ (Eq. (28)). This power-law index is very close to that of the evolution due to stellar encounters in Equation (30), which is -1.4.

4.2. Planetesimal Disks with a_0 -Distribution

We show the evolution and lifetime of disks that consist of planetesimals with a_0 -distribution and several additional effects.

4.2.1. Decay of Comet Clouds

Figure 12 shows P_{bound} for the disks with $\gamma = -2$ and 0 (W0 and W1). The e -folding time obtained by fitting are 15.9 Gyr and 5.2 Gyr for $\gamma = -2$ and 0, respectively. We approximate the decay of the planetesimal number for the disk with a_0 -distribution using $P_{\text{bound}}^{\text{fit}}$ for the planetesimal disk of identical a_0 . The decay curve for the disk with a_0 -distribution is obtained by averaging $P_{\text{bound}}^{\text{fit}}$ (eq. (29) or (31)) over a_0 but it cannot be obtained analytically. Therefore, we estimate the decay curve by averaging Equation (30) instead of Equation (29). We assume that planetesimals have a_0 -distribution following $dn/da_0 \propto a_0^\gamma$ in the range of $5 \times 10^3 - 5 \times 10^4$ AU. Integrating Equation (30) over a_0 using the probability density distribution of a_0 that is proportional to dn/da_0 , we obtain the averaged e -folding time $\langle t_e \rangle$ 17.9 Gyr, 6.7 Gyr, and 3.9 Gyr for $\gamma = -2$, 0, and 1 (W0, W1, and W2. See Table 2), respectively. They are slightly shorter than the e -folding times obtained by fitting. The agreements of P_{bound} and $P_{\text{bound}}^{\text{fit}}$ shown in Figure 12 are reasonably good as well as those for the identical a_0 models (Fig. 8).

4.2.2. Evolution of the disk structure

Figure 13 shows the time evolution of r -distributions for the disks W0 and W1, respectively. The disk W0 keeps the initial distribution during the evolution. On the other hand, the r -distribution for the disk W1 greatly changes and approaches that with $\gamma \simeq -2$ where we assume that the disks have the r -distributions that follow $dn/dr \propto r^\gamma$. Figure 13

shows the r -distributions in 10 Gyr for all the disk models. All the distribution in 10 Gyr are close to $dn/dr \propto r^{-2}$. Rickman et al. (2008) also found in the calculation that the disk initially with $\gamma = -1.5$ evolves into a distribution with $\gamma \simeq -2$. The final r -distributions with $\gamma = -2$ can be explained as follows: The energy kicks that are small but repeatedly given by stars, relax the initial energy distribution and result in a wide and smooth energy distribution whose width is larger than the energy range of the Oort cloud. Therefore, when applied to the narrow energy range of the Oort cloud, the energy distribution is roughly flat, from which follows $dn/da \propto a^{-2}$ (Mal'ushkin & Tremaine 1999). Using $a \propto r$, we expect r -distribution follows $dn/dr \propto r^{-2}$.

Next, we divide the disk evenly by r and see how the disk evolves into a spherical structure from a flat disk. To evaluate this structural evolution, we introduce a new index α_r , which is a normalized ratio of the sums of the square of the vertical axis and the radial axis defined by

$$\alpha_r = \frac{\Sigma z^2}{\Sigma (x^2 + y^2)}, \quad (35)$$

where x, y, z are the coordinates that satisfy $r^2 \leq x^2 + y^2 + z^2 < (r + \Delta r)^2$. When the structure between r and $r + \Delta r$ is perfectly flat, $\alpha_r = 0$. The r -dependence of α_r for W0 is plotted in Figure 14 at various times, showing the evolution of the flat disk into the spherical cloud. Since the flare-up of the disk occurs contiguously with r and time, it is difficult to tell from this figure where the boundary of the inner (relatively flat) and outer (spherical and isotropic) Oort clouds is. The high α_r at $r < 5 \times 10^3$ AU is due to new comets injected from the outer Oort cloud.

Figure 14 shows the r -dependence of α_r for the model with the Galactic tide (W3). We can see that the Galactic tide (1) accelerates the flare-up of the disk, especially at the beginning, and (2) produces a wave-like structure propagating inward. The wave is due to the nature of the Galactic tide that causes a periodic oscillation of the inclinations against

the Galactic plane ($i = 63^\circ$). Therefore all planetesimals follow similar orbital evolution with different timescales that depend on the orbital elements (especially on a). The effect of passing stars is too weak to let planetesimals forget their conservative quantities completely within the timescale of the oscillation due to the Galactic tide. However, their inclinations do not have an isotropic distribution even for $\alpha = 0.5$ since the Galactic tide does not randomize the orbital elements of planetesimals. Due to the wave, it is difficult to distinguish the inner and outer Oort clouds using α_r in W3.

4.2.3. Radial transport of planetesimals

We calculate the decay of planetesimals in each r range $P_{\text{bound}}(r)$ and derive their fits. However, due to the radial transport of planetesimals, not all $P_{\text{bound}}(r)$ decay monotonically. We deal with only r -bins whose $P_{\text{bound}}(r)$ shows a monotonic decay. For W0, $P_{\text{bound}}(r)$ only $r < 8 \times 10^4 \text{AU}$ shows a monotonic decay, while P_{bound} for $r > 8 \times 10^4 \text{AU}$ region shows an increase in the number of planetesimals due to the outward transport of planetesimals. Assuming that the decay curves follow the standard exponential and Kohlrausch formula, we calculate t_e , t_0 , and β for $r < 10^5 \text{AU}$ by fitting. Also for the r -bins that do not have a monotonic decay, we obtain t_e , t_0 , and β using the decreasing part of P_{bound} .

First, we compare the results for disks with different γ (models W0 and W1). Figure ?? shows averaged t_e and t_0 obtained by the fitting of numerical results with error bars against r . For $\gamma = -2$, t_e and t_0 are almost flat at $t_e \sim t_0 \sim 10 \text{ Gyr}$ for any r . In contrast, t_e and t_0 for $\gamma = 0$ decrease inversely proportionally to r . This indicates that the efficiency of the planetesimal supply from the inner Oort cloud to the outer Oort cloud strongly depends on the a_0 -distribution. The dependence of $t_e \propto r^{-1}$ corresponds to Equation (7) derived under an assumption that a -distribution is constant (i.e., no planetesimal supply). Figure ?? also shows β obtained by fitting. We find that W0 and W1 have $\beta > 1$ for the inner Oort cloud

and $\beta < 1$ for the outer Oort cloud (see 4.1.2). This means that no matter how massive the outer Oort cloud is, the net rate of transportation of comets due to the perturbation from stars is outward.

Second, we compare the evolution for the disk W0 to those under the Galactic tide and non-identical stars (W3 and W4) in Figure ???. In general, the effects of the Galactic tide and the non-identical stars are small although the error bars in model W4 are much larger than those for the other disks. But in detail, we can see that the Galactic tide increases t_e and t_0 and reduces β . This slight stabilization may be due to the decrease of mean heliocentric distances of planetesimals, $a(1 + e^2/2)$, as a result of the decrease of e of planetesimals that are in the Kozai-Lidov cycle. In the Kozai-Lidov cycle, the eccentricity of most of the planetesimals initially with $e \simeq 1$ decreases (Higuchi et al. 2007).

5. SUMMARY AND DISCUSSION

We have investigated the effect of stellar encounters on Oort cloud formation from a flat disk to a spherical structure. First we analytically derived the impact parameters for e , i , and ω changes and compared them to the impact parameter for ejection using the classical impulse approximation. Using these impact parameters, we showed that the relaxation timescale for i is much shorter than those for e , ω and ejection and e does not evolve according to a normal random walk but a Lévy flight.

Next, we performed numerical calculations of the evolution of planetesimal disks by stellar encounters using the classical impulse approximation. We numerically and analytically showed that the encounter with distant stars is not effective, either in ejection of planetesimals or in randomization of the orbital elements. We empirically derived the fitting formulae $P_{\text{bound}}^{\text{fit}}$ using the standard exponential formula and the Kohlrausch formula. We obtained the timescales t_e and t_0 and the stretching parameter β for the disk that consists of planetesimals with identical initial semimajor axis a_0 and the local t_e , t_0 , and β as functions of the heliocentric distance r . Using t_e , t_0 , and β , we discussed the timescale and efficiency of transporting of comets from the inner/outer Oort cloud. We found that the timescale of the decay of the Oort cloud is almost the same at any r , as seen in the r -distribution that follows $dn/dr \propto r^{-2}$ during evolution. This is due to the sufficient supply of planetesimals from the inner Oort cloud to the outer Oort cloud. If the initial planetesimal disk has a relatively outer-massive distribution and the outward supply of planetesimals is small, the outer Oort cloud has a much shorter lifetime roughly proportional to r^{-1} . We found that, in any disk model, the decay rate of the outer Oort cloud is smaller than the standard exponential decay rate ($\beta \lesssim 1$) because of the sufficient supply of planetesimals from the inner Oort cloud. We showed that the distribution of the semimajor axes of comets in the Oort cloud approximately follows $dn/da \propto a^{-2}$ for any

initial distribution of the semimajor axis. This corresponds to the flat distribution of orbital energies. Since the initial a -distribution of the scattered planetesimal disk generated by planet scattering follows $dn/da \propto a^{-2}$ as shown in Higuchi et al. (2007), the a -distribution of the Oort cloud does not change during evolution.

The local Galactic environment in the stage of Oort cloud formation such as stellar parameters and the distance from the Galactic center and the Galactic potential could be different from the current one used in our simulations (e.g., Brasser & Schwamb 2010, 2014). As discussed in Brasser et al. (2006), if the Solar system spent in a cluster embedded in a giant molecular cloud just after it formed, the high density of the cluster accelerates the evolution of the Oort cloud. Investigation of the time evolution of the Galactic environment is left for future work.

The distribution of the orbital elements, especially i of new comets produced by the Galactic tide is an interesting subject that is directly connected to observations. Our study showed that the timescales of the evolution due to stellar encounters is analytically proportional to a_0^{-1} (Eq. 7) and numerically proportional to $a_0^{-1.4}$ (Eq. 30 and independent of r (Fig. ??). As the timescale of the evolution due to the Galactic tide is proportional to $a^{-3/2}$ (Eq. 28), the difference of the effects of stellar encounters and the Galactic tide might be seen especially in the anisotropic i - distribution of the new comets against their original semimajor axes. The production and the distribution of new comets will be the subject of our next work.

A. Initial a -Distribution of Planetesimals

Higuchi et al. (2006) numerically showed that the probability distribution function for the Oort cloud comet candidates formed by planetary scattering (i.e., widely distributed scattered planetesimal disk) is

$$P(a > a_c) \propto a_c^{-1}, \quad (\text{A1})$$

where a_c is the minimum semimajor axis for the Oort cloud comet candidates. This is valid for $a_c \gtrsim 10a_{\text{planet}}$, where a_{planet} is the semimajor axis of the planet that formed the Oort cloud comet candidates by planetesimal scattering. This function means the scattering process of planetesimals by a planet is a Lévy flight (e.g., Mandelbrot 1982). Equation (A1) shows that the distribution of the semimajor axes follows,

$$\frac{dn}{da} \propto a^{-2}, \quad (\text{A2})$$

which corresponds to the energy distribution

$$\frac{dn}{dE} = \text{const.}, \quad (\text{A3})$$

where $E = 1/a$. This uniform distribution can be explained using a Gaussian energy kick distribution. If the distribution of the energy kick given by a planet follows a Gaussian distribution the energy distribution of planetesimals is

$$\frac{dn}{dE} \propto \exp [-(E - E_0)^2], \quad (\text{A4})$$

where $E_0 = 1/a_0$ and a_0 is the semimajor axis of the planetesimal before planetary scattering. The energy range for Oort cloud comets is very narrow and close to $E = 0$, which means the Oort cloud energy range lies on the low-energy tail of the Gaussian energy distribution. The gradient of the distribution is given by

$$\left(\frac{d}{dE} \right)^2 n \propto -2(E - E_0) \exp [-(E - E_0)^2], \quad (\text{A5})$$

which goes to zero when $E_0 \gg E$ and $E \rightarrow 0$. This means that $\gamma = -2$ is expected.

B. Effect of Distant Stars

We analytically derive the effect of passing stars with $b_p > b_{\text{esc}}$, which does not eject planetesimals by a single encounter. Assuming that the initial velocity of a planetesimal v is much smaller than Δv , the energy change per unit mass due to a stellar encounter is given as $\Delta E \sim \frac{1}{2}(\Delta v)^2$. Then the energy change given by stars for $b_{\text{min}} < b < b_{\text{max}}$ per unit time is

$$\Delta E_t = \int_{b_{\text{min}}}^{b_{\text{max}}} 2\pi b f \Delta E db, \quad (\text{B1})$$

where f is a flux of stars per unit area per unit time (i.e., $f = f_{\text{enc}} \pi^{-1} \text{Myr}^{-1}$). Assuming $b_p \ll b$ in Equation (1), we have $\Delta E \propto b^{-4}$. This means that ΔE_t converges with $b \rightarrow \infty$.

To compare the effects of stars that do not penetrate the Oort cloud and that penetrate it (but not close enough to eject a comet by a single encounter), we evaluate these effects as a function of r . The averaged energy change per unit time given by random stellar encounters for $b_{\text{esc}} < b < \infty$ is given by

$$\langle \Delta E_t \rangle = \frac{1}{\pi} \int_0^1 \int_0^\pi \int_{b_{\text{esc}}}^\infty 2\pi b f \Delta E db d\beta d\cos\alpha, \quad (\text{B2})$$

where α and β are the direction angles of stellar encounters and $\cos\alpha$ and β have uniform distributions. We integrate Equation (B2) neglecting the small terms and avoiding the region where a single stellar encounter ejects comets (see Appendix. C). Then we have

$$\Delta E_t = \frac{4\pi G^2 m_*^2 f}{v_*^2} \Theta_j, \quad (j = 1, 2, 3) \quad (\text{B3})$$

$$\Theta_1 \sim \ln \eta, \quad [b < r - b_{\text{esc}}] \quad (\text{B4})$$

$$\Theta_2 \sim \frac{\sqrt{2}(2+\pi)}{\pi} \eta^{-\frac{1}{4}}, \quad [r - b_{\text{esc}} < b < r + b_{\text{esc}}] \quad (\text{B5})$$

$$\Theta_3 \sim 1 - \pi \sqrt{2} \eta^{-\frac{1}{4}}, \quad [r + b_{\text{esc}} < b] \quad (\text{B6})$$

where $\eta = r/(m_*/v_*)^2 M_\odot / 2G = r^2/b_{\text{esc}}^2$. For $m_* = 0.5M_\odot$ and $v_* = 20 \text{kms}^{-1}$, $\eta \gg 1$.

Assuming r as the radius of the Oort cloud, we can say that Equations (B4) and (B5) are for

stellar encounters penetrating the Oort cloud ($b < r + b_{\text{esc}}$), and Equation (B6) is for that not penetrating ($b > r + b_{\text{esc}}$). We also numerically integrate Equation (B2) for $b_{\text{min}} = b_{\text{esc}}$ and $b_{\text{max}} = 1$ pc and find that Equations (B4)-(B6) are good approximations within $\sim 20\%$ error for $r \geq 10^4$ AU. Since the ratio $(\Theta_1 + \Theta_2)/\Theta_3 > 10$ for any r for $m_* = 0.5M_\odot$ and $v_* = 20 \text{ kms}^{-1}$ (i.e., $\eta \simeq r$), we conclude that the effect of stars not penetrating the Oort cloud is small.

C. Integration of Equation (B2)

To perform the integration of Equation (B2), we introduce coordinates similar to Baily (1983); centered on the Sun with z -axis parallel to \mathbf{v}_* and choose the x -axis so that \mathbf{r} is on the x - z plane. The last axis in the left-handed coordinate system is the y -axis. Then \mathbf{b} is on the x - y plane. Let the angle between \mathbf{r} and y -axis α and the angle between \mathbf{b} and x -axis β . When the direction angle of stellar encounters is isotropic, $\cos \alpha$ and β have uniform distributions between -1 and 1 and 0 and 360° , respectively. The stellar impact parameters against the Sun \mathbf{b} and a planetesimal \mathbf{b}_p are

$$\mathbf{b} = \begin{pmatrix} b \cos \beta \\ b \sin \beta \\ 0 \end{pmatrix}, \quad (\text{C1})$$

$$\mathbf{b}_p = \begin{pmatrix} b \cos \beta - r \sin \alpha \\ b \sin \beta \\ 0 \end{pmatrix}. \quad (\text{C2})$$

Equation (1) is rewritten as

$$\Delta \mathbf{v} = \frac{2Gm_*}{v_*} \begin{pmatrix} \frac{b \cos \beta - r \sin \alpha}{D^2} - \frac{b \cos \beta}{b^2} \\ \frac{b \sin \beta}{D^2} - \frac{b \sin \beta}{b^2} \\ 0 \end{pmatrix}, \quad (\text{C3})$$

where

$$D^2 = b^2 + r^2 \sin^2 \alpha - 2br \sin \alpha \cos \beta. \quad (\text{C4})$$

The averaged energy change per unit times given by stellar encounters are given by Equation (B2). We avoid the range $b_p \leq b_{\text{esc}}$ from the integral where a single energy kick is large enough to eject a planetesimal. Then b is divided into three ranges: (1) $[b_{\text{esc}}, r - b_{\text{esc}}]$, (2) $[r - b_{\text{esc}}, r + b_{\text{esc}}]$, and (3) $[r + b_{\text{esc}}, \infty]$. We integrate Equation (B2) by neglecting the $(b_{\text{esc}}/b)^2$ terms and using $\eta \gg 1$ and obtained the following formulae for each b range,

$$\Delta E_t = \frac{4\pi G^2 m_*^2 f}{v_*^2} \Theta_j \quad (j = 1, 2, 3) \quad (\text{C5})$$

$$\begin{aligned} \Theta_1 &\simeq \left(2\sqrt{2} - \frac{\sqrt{2}}{2} \ln \eta \right) \eta^{-\frac{1}{4}} - \frac{2}{\pi} \eta^{-\frac{1}{2}} + \ln \left[\frac{4\eta^{3/2}}{(\eta - 1)^{1/2}} \left(\frac{1 - \sqrt{2}\eta^{-\frac{1}{4}}}{1 + \sqrt{2}\eta^{-\frac{1}{4}}} \right) \right] - 2 + \frac{1}{\pi} \\ &\sim \ln \eta \end{aligned} \quad [b < r - b_{\text{esc}}] \quad (\text{C6})$$

$$\begin{aligned} \Theta_2 &\simeq \frac{2\sqrt{2}}{\pi} \eta^{-\frac{5}{4}} + 2\sqrt{2} \eta^{-\frac{3}{4}} + \frac{\sqrt{2}(2 + \pi)}{\pi} \eta^{-\frac{1}{4}} + 2 \ln \frac{1 + \eta^{-1/2}}{1 - \eta^{-1/2}} \\ &\sim \frac{\sqrt{2}(2 + \pi)}{\pi} \eta^{-\frac{1}{4}} \end{aligned} \quad [r - b_{\text{esc}} < b < r + b_{\text{esc}}] \quad (\text{C7})$$

$$\begin{aligned} \Theta_3 &\simeq 1 - \sqrt{(1 + \eta^{-1/2})^2 - 1} \arcsin [(1 + \eta^{-1/2})^{-1}] \\ &\sim 1 - \frac{\pi}{\sqrt{2}} \eta^{-\frac{1}{4}}. \end{aligned} \quad [r + b_{\text{esc}} < b] \quad (\text{C8})$$

We are grateful to an anonymous referee for a number of helpful comments that allowed us to improve the manuscript. We also thank Ramon Brasser for valuable discussions, especially during the revising process. Data analysis were in part carried out on PC cluster at Center for Computational Astrophysics, National Astronomical Observatory of Japan.

REFERENCES

- Allen, C. 1985 *Astrophysical Quantities*, 3rd edn. Athlone Press, London
- Baily, M. E. 1983, *MNRAS*, 204, 603
- Binney, J. & Tremaine, S. 1987, *Galactic Dynamics*, Princeton: Princeton University Press
- Brasser, R., Duncan, M., & Levison, H. F. 2006, *Icarus* 184, 59
- Brasser, R., Higuchi, A., & Kaib, N. 2010, *A&A*, 516, 12
- Brasser, R. & Schwamb, M. E. 2014, *MNRAS*, Accepted
- Byl, J. 1986, *Earth Moon Planets*, 36, 263
- Collins, B. F. & Sari, R. 2008, *AJ*, 136, 2552
- Dones, L., Weissman, P., Levison, H. F., & Duncan, M. 2004 In *Comet II*
- Dobrovolskis, A. R., Alvarellos, J. L., & Lissauer, J. J. 2007 *Icarus*, 188, 481
- Duncan, M., Quinn, T. & Tremaine, S. 1987, *AJ*, 94, 1330
- Dybczyński, P. A. 2002, *A&A*, 396, 283
- Fernandéz, J. A. 1997, *Icarus*, 129, 106
- Fernandéz, J. A. & Brunini, A. 2000, *Icarus*, 145, 580
- Fouchard, M., Froeschlé, Ch., Rickman, H., & Valsecchi, G. B. 2011, *Icarus*, 214, 334
- García-Sánchez, J., Weissman, P. R., Preston, R. A., Jones, D. L., Lestrade, J.-F., Latham, D. W., Stefanik, R. P. & Paredes, J. M. 2001 *A&A*, 379, 634
- Harrington, R. S. 1985 *Icarus*, 61, 60

- Heisler, J. & Tremaine, S. 1986, *Icarus*, 65, 13
- Heisler, J., Tremaine, S., & Alcock, C. 1987, *Icarus*, 70, 269
- Higuchi, A., Kokubo, E., & Mukai, T. 2006, *AJ*, 131, 1119
- Higuchi, A., Kokubo, E., Kinoshita, H., & Mukai, T. 2007, *AJ*, 134, 1693
- Holmberg, J.& Flynn, C. 2000, *MNRAS*, 313, 209
- Hut, P. & Tremaine, S. 1985, *AJ*, 90, 1548
- Kinoshita, H & Nakai, H. 1999, *Celestial Mechanics and Dynamical Astronomy*. 75, 125
- Kokubo, E., Yoshinaga, K., & Makino, J. 1998, *MNRAS*, 297, 1067
- Kozai, Y. 1962, *AJ*, 67, 591
- Malyshkin, L. & Tremaine, S. 1999, *Icarus*, 141, 341
- Mandelbrot, B. B. 1982, *The Fractal Geometry of Nature* (Updated and augm. ed.). New York: W. H. Freeman. ISBN 0-7167-1186-9
- Murray, C. D.& Dermott, S. F. 1999, *Solar System Dynamics*, Cambridge: Cambridge University Press
- Oort, J. H 1950, *Bull. Astron. Inst. Netherlands*, 11, 91
- Rickman, H. 1976 *Bull. Astron. Inst. Czech.* 27, 92
- Rickman, H., Froeschlé, Ch., Froeschlé, Cl., & Valsecchi, G. B. 2004, *A&A*, 428, 673
- Rickman, H., Fouchard, M., Valsecchi, G. B., & Froeschlé, Ch. 2005, *Earth, Moon, and Planets*. 97, 411

- Rickman, H., Fouchard, M., Froeschlé, Ch., & Valsecchi, G. B. 2008, *Celestial Mechanics and Dynamical Astronomy*. 102, 111
- Tremaine, S., 1993, *Planets around pulsars; Proceedings of the Conference, California Inst. of Technology, Pasadena*, 335
- Weinberg, M. D., Shapiro, S. L., & Wasserman, I. 1987, *ApJ*, 312, 367
- Weissman, P. R. 1980, *Nature*, 288, 242
- Weissman, P. R. 1990, *Nature*, 344, 825

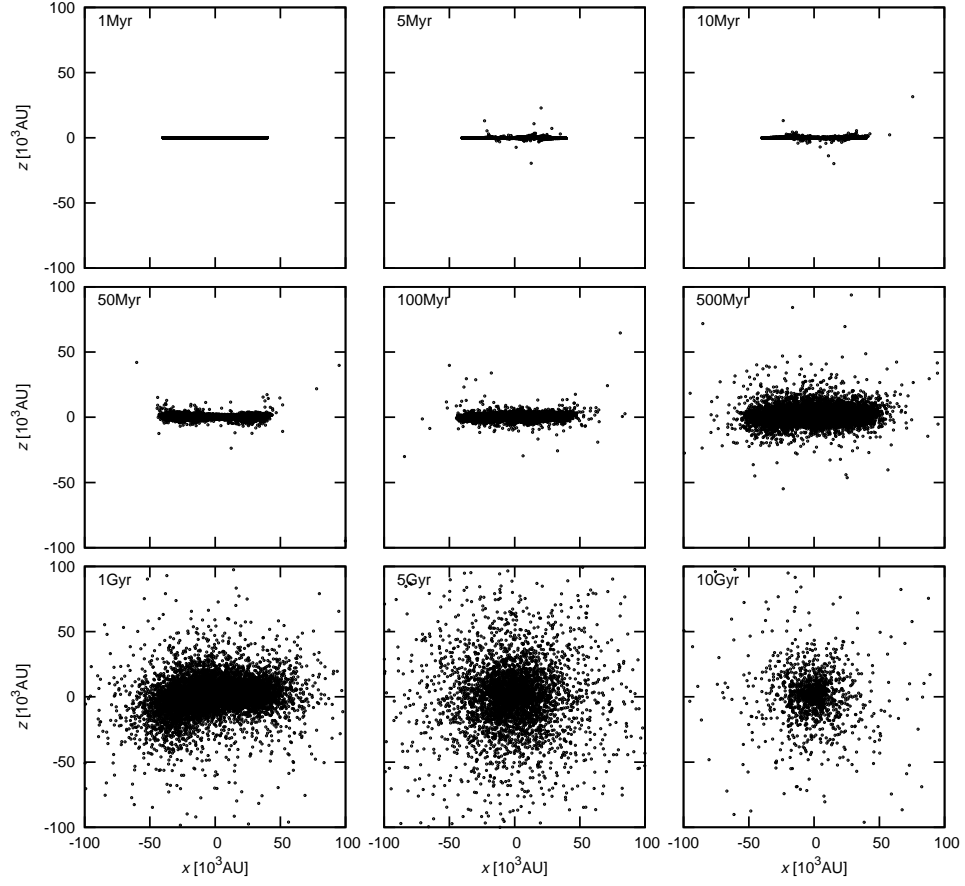


Fig. 1.— Snapshots on the x - z for model I0 of $a_0 = 2 \times 10^4$ AU at $t = 1$ Myr, 5 Myr, 10 Myr, 50 Myr, ... , and 10 Gyr.

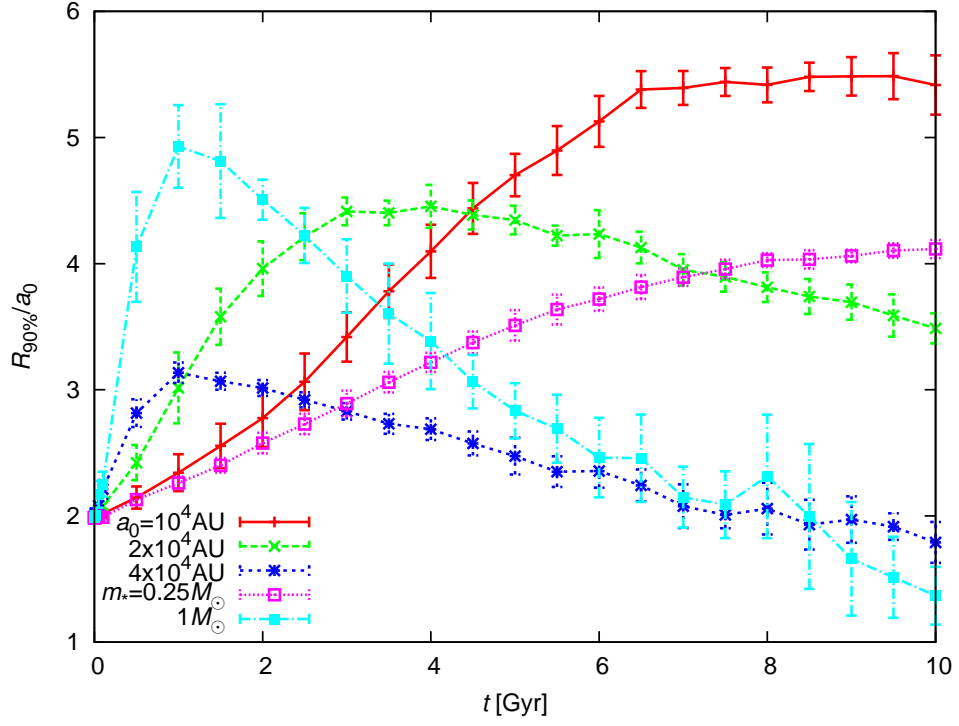


Fig. 2.— Disk radius $R_{90\%}$ that contains 90 percent of planetesimals inside it against t for model I0 of $a_0 = 2 \times 10^4$ AU and $m_* = 0.5 M_\odot$ (solid), $a_0 = 2 \times 10^4$ AU and $m_* = 0.5 M_\odot$ (dashed), $a_0 = 2 \times 10^4$ AU and $m_* = 0.5 M_\odot$ (short-dashed), $a_0 = 2 \times 10^4$ AU and $m_* = 0.25 M_\odot$ (dotted), and $a_0 = 2 \times 10^4$ AU and $m_* = 1 M_\odot$ (dot-dashed).

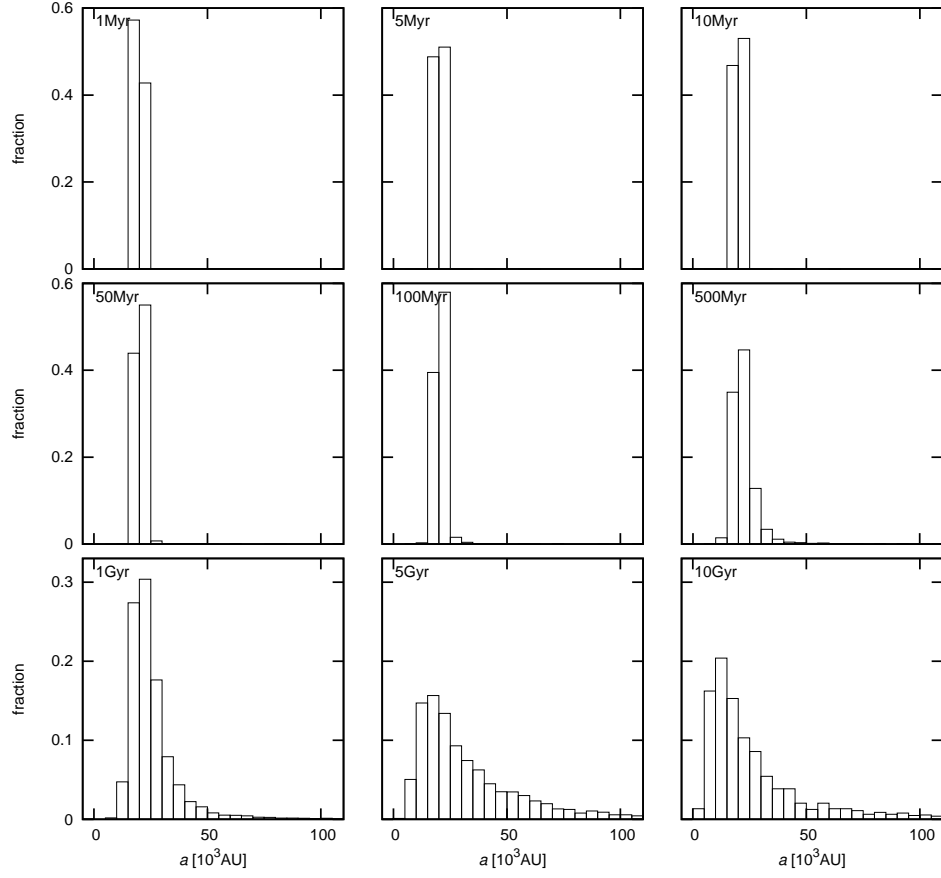


Fig. 3.— Normalized distributions of semimajor axes for model I0 of $a_0 = 2 \times 10^4 \text{ AU}$ at $t = 1 \text{ Myr}$, 5 Myr , 10 Myr , 50 Myr , ... , and 10 Gyr .

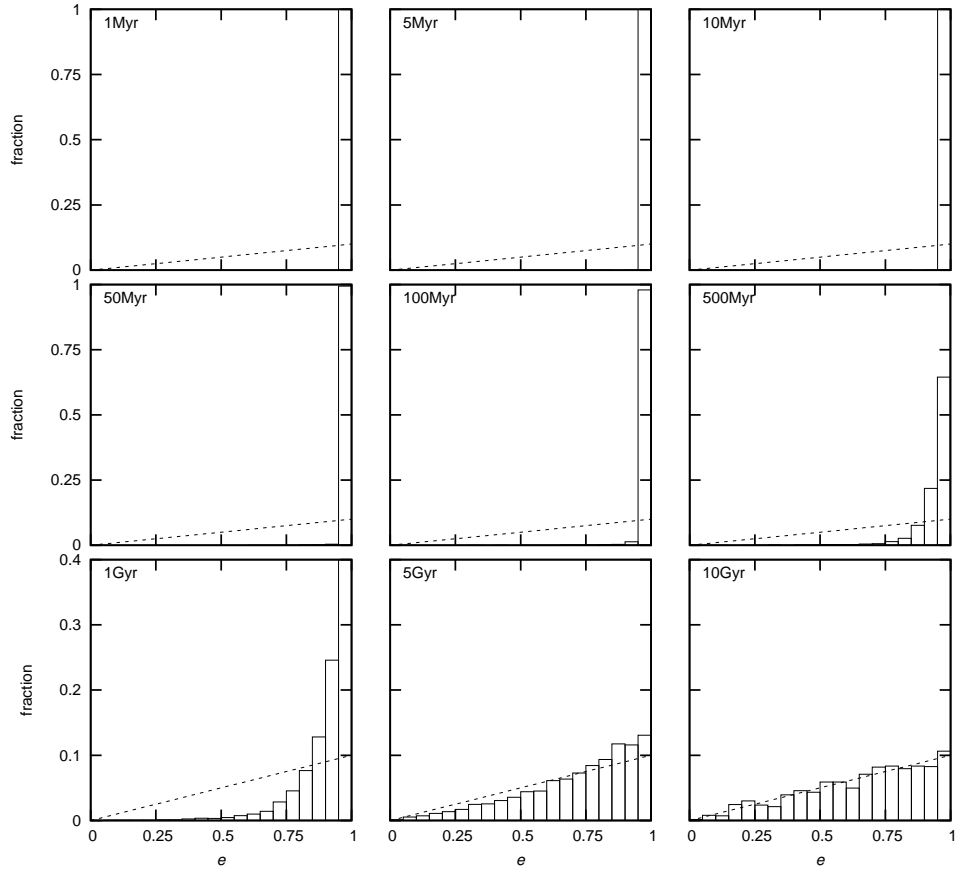


Fig. 4.— Same as Fig.3 but for eccentricity. The short-dashed lines show the isotropic distribution.

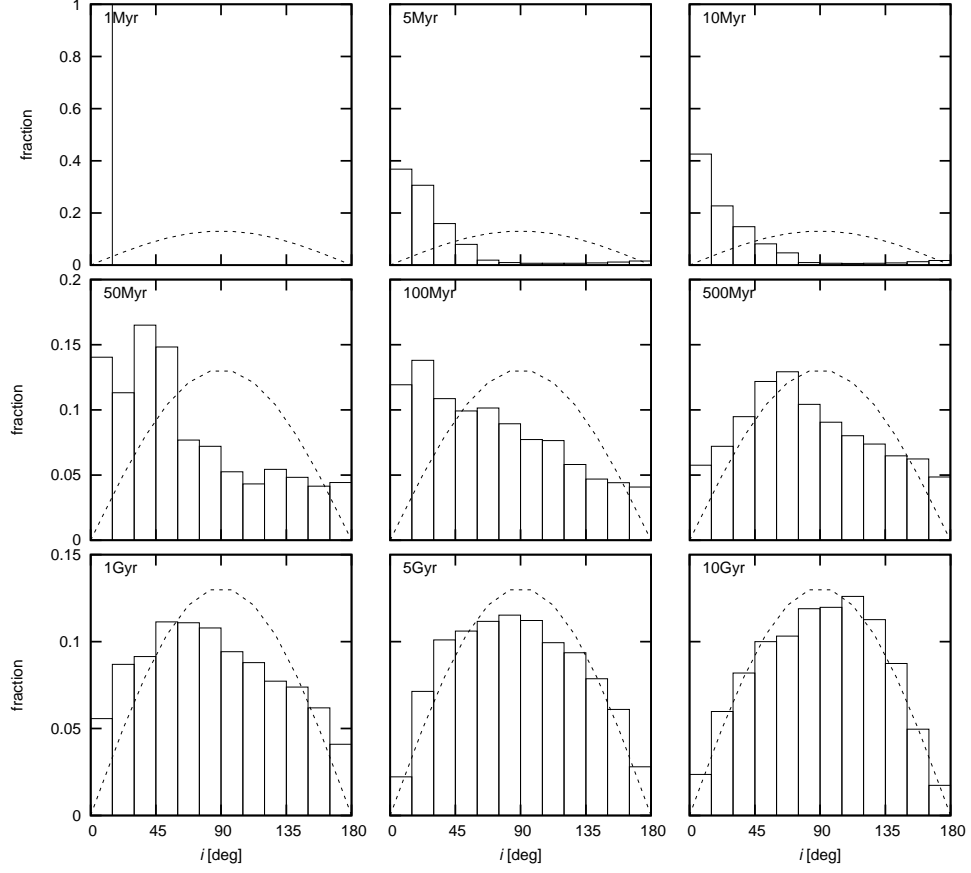


Fig. 5.— Same as Fig.3 but for inclination. The short-dashed curves show the isotropic distribution.

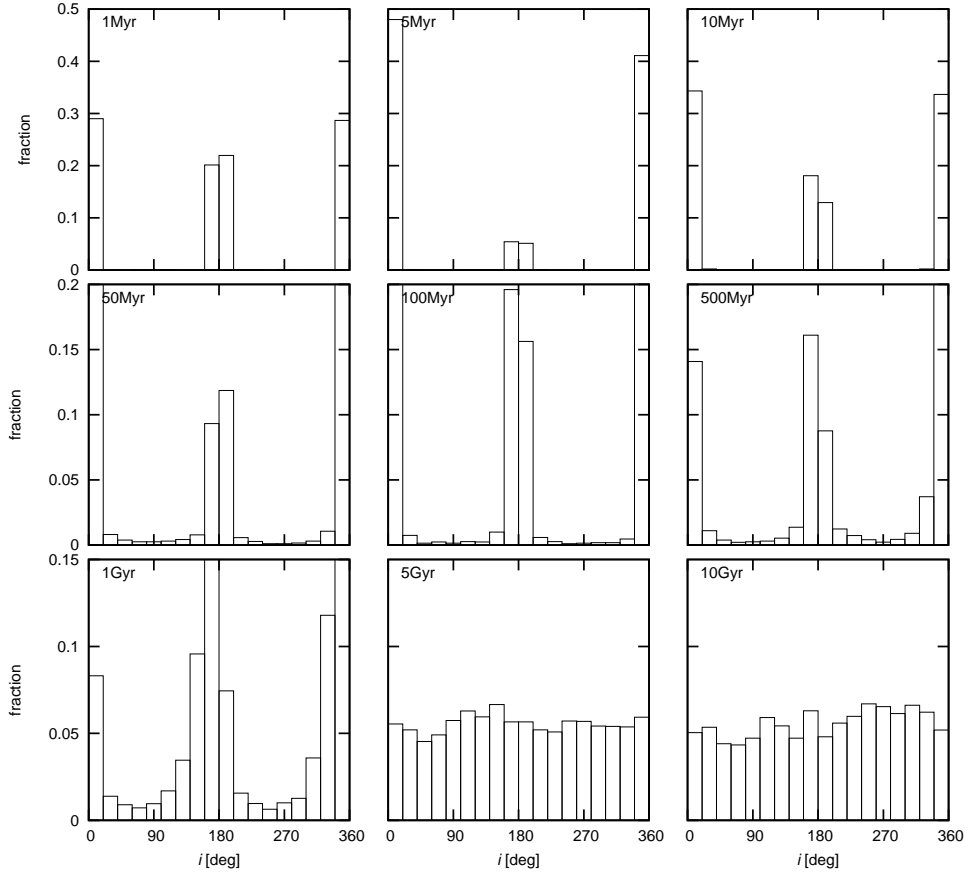


Fig. 6.— Same as Fig.3 but for argument of perihelion.

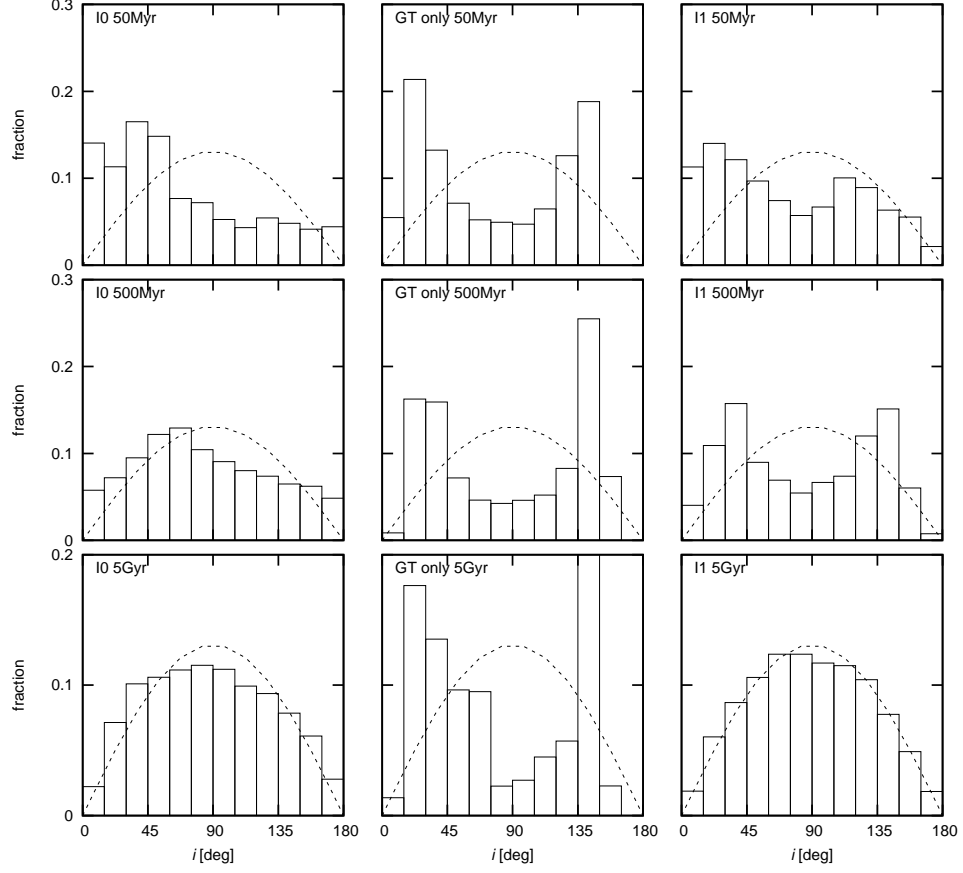


Fig. 7.— Evolution of inclination distribution due to passing stars only (left, model I0), the Galactic tide only (middle), and both of them (right, model I1) at 50 Myr, 500 Myr, and 5 Gyr for $a_0 = 2 \times 10^4$ AU.

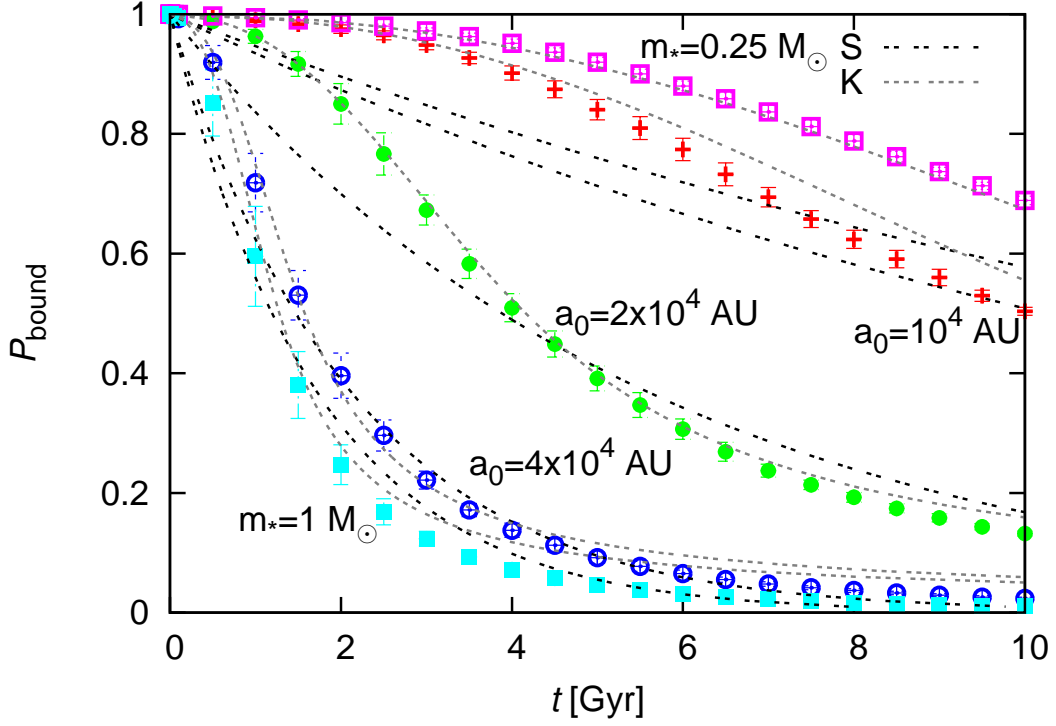


Fig. 8.— Surviving rate of planetesimals P_{bound} with $1\text{-}\sigma$ error bars against t for model I0 of $a_0 = 10^4 \text{ AU}$ and $m_* = 0.5 M_\odot$ (crosses), $a_0 = 2 \times 10^4 \text{ AU}$ and $m_* = 0.5 M_\odot$ (circles), $a_0 = 4 \times 10^4 \text{ AU}$ and $m_* = 0.5 M_\odot$ (open circles), $a_0 = 2 \times 10^4 \text{ AU}$ and $m_* = 0.25 M_\odot$ (open squares), and $a_0 = 2 \times 10^4 \text{ AU}$ and $m_* = 1 M_\odot$ (squares) with $P_{\text{bound}}^{\text{fit}}$ using the standard exponential decay (S, double short-dashed curve) and the stretched exponential decay (K, dotted curve).

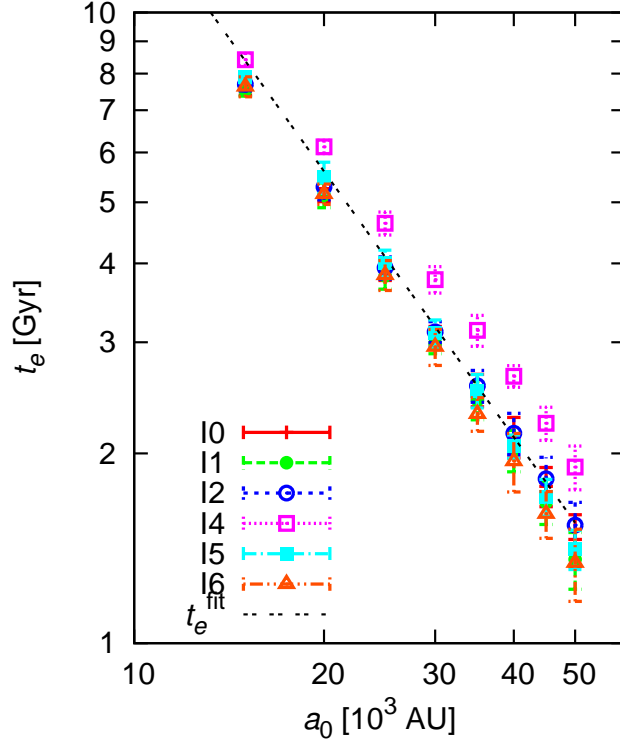


Fig. 9.— e -folding time t_e with $1\text{-}\sigma$ error bars against a_0 for models I0 (crosses), I1 (circles), I2 (open circles), I4 (open squares), I5 (squares), and I6 (open triangles) with t_e^{fit} (double short-dashed line).

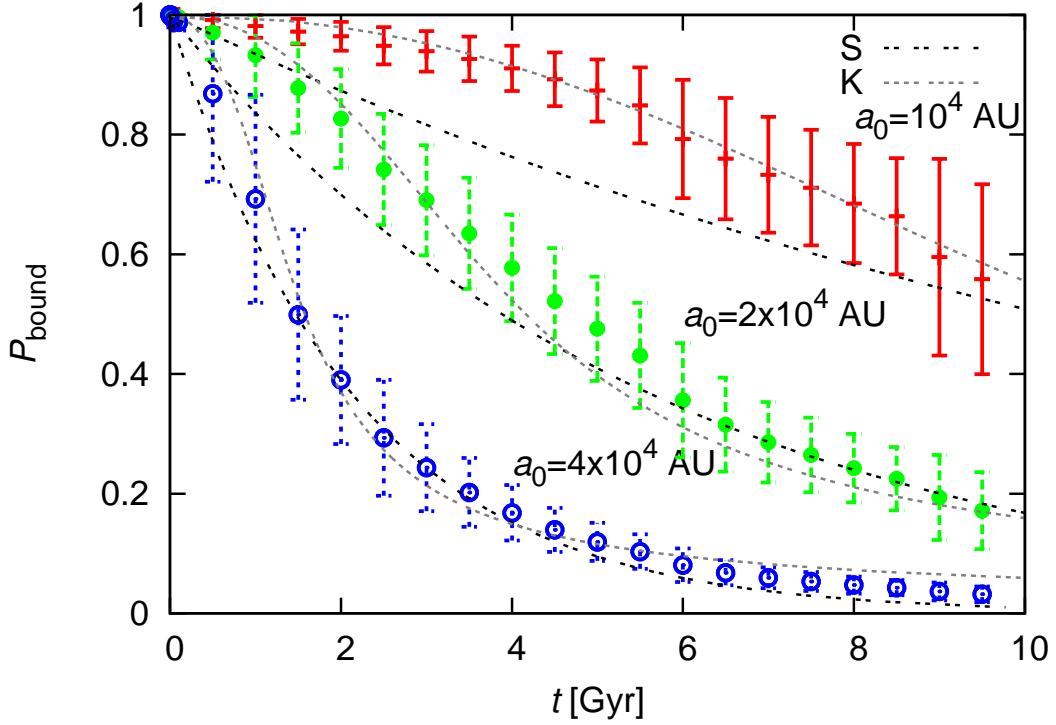


Fig. 10.— Surviving rate of planetesimals P_{bound} due to encounters with non-identical mass stars (model I3) with $1\text{-}\sigma$ error bars for model I3 of $a_0 = 10^4 \text{ AU}$ and $m_* = 0.5 M_\odot$ (crosses), $a_0 = 2 \times 10^4 \text{ AU}$ and $m_* = 0.5 M_\odot$ (circles), and $a_0 = 4 \times 10^4 \text{ AU}$ and $m_* = 0.5 M_\odot$ (open circles) against t with $P_{\text{bound}}^{\text{fit}}$ for $m_* = 0.5 M_\odot$ using the standard exponential decay (S, double short-dashed curve) and the stretched exponential decay (K, dotted curve).

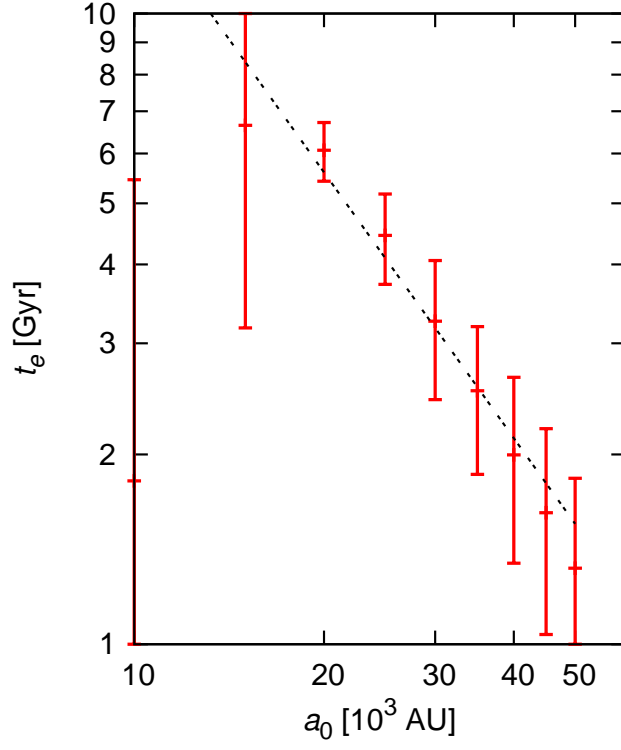


Fig. 11.— e -folding time t_e against a_0 with $1\text{-}\sigma$ error bars for the non-identical mass star model (model I3) and t_e^{fit} for $m_* = 0.5M_\odot$ (double short-dashed line).

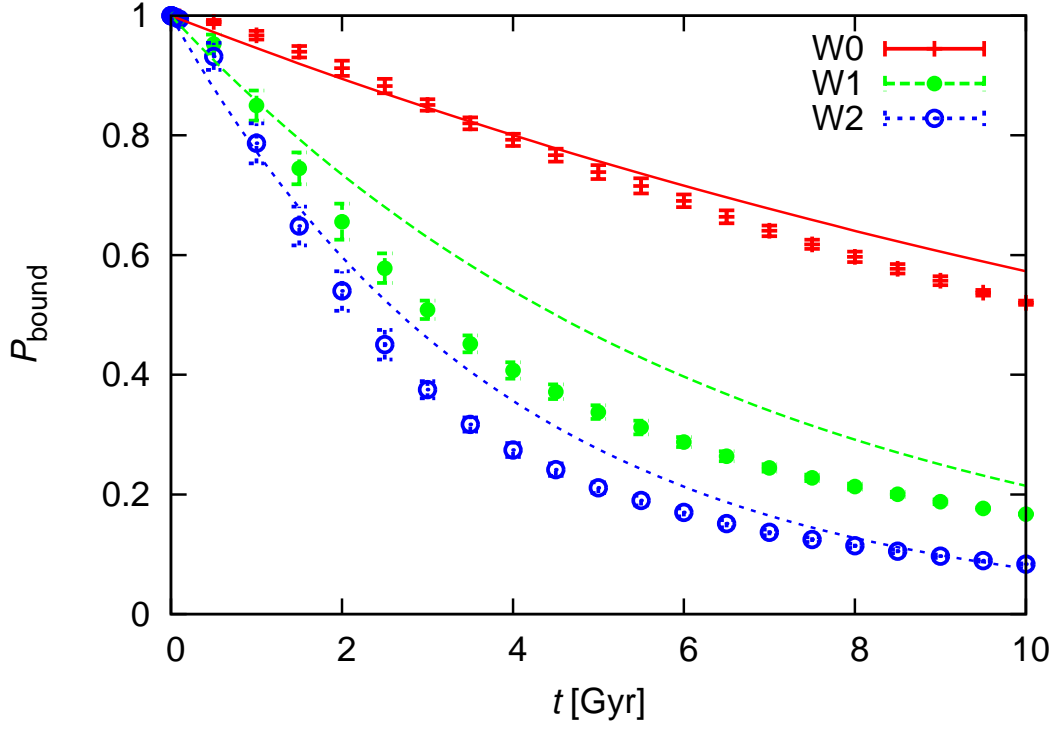


Fig. 12.— Surviving rate of planetesimals P_{bound} against t for models W0 (crosses), W1 (circles), and W2 (open circles) with 1- σ error bars and $P_{\text{bound}}^{\text{fit}}$ using $\langle t_e \rangle$ for W0 (solid curve), W1 (dashed curve), and W2 (short-dashed curve).

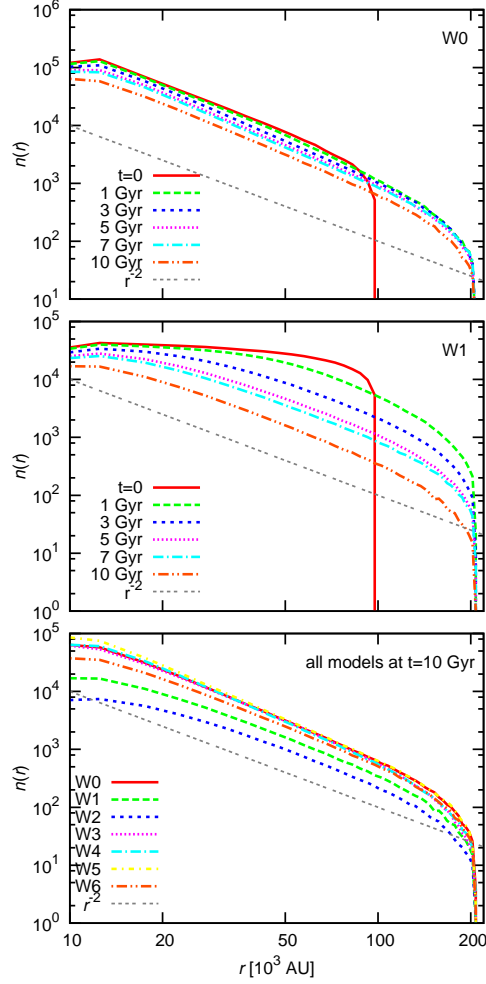


Fig. 13.— Time evolution of distributions of heliocentric distances for models W0 (top) and W1 (middle). The vertical axis shows the number of planetesimals in each r -bin. Distributions of heliocentric distances at $t = 10$ Gyr for all the models summarized in Table 2 (bottom).

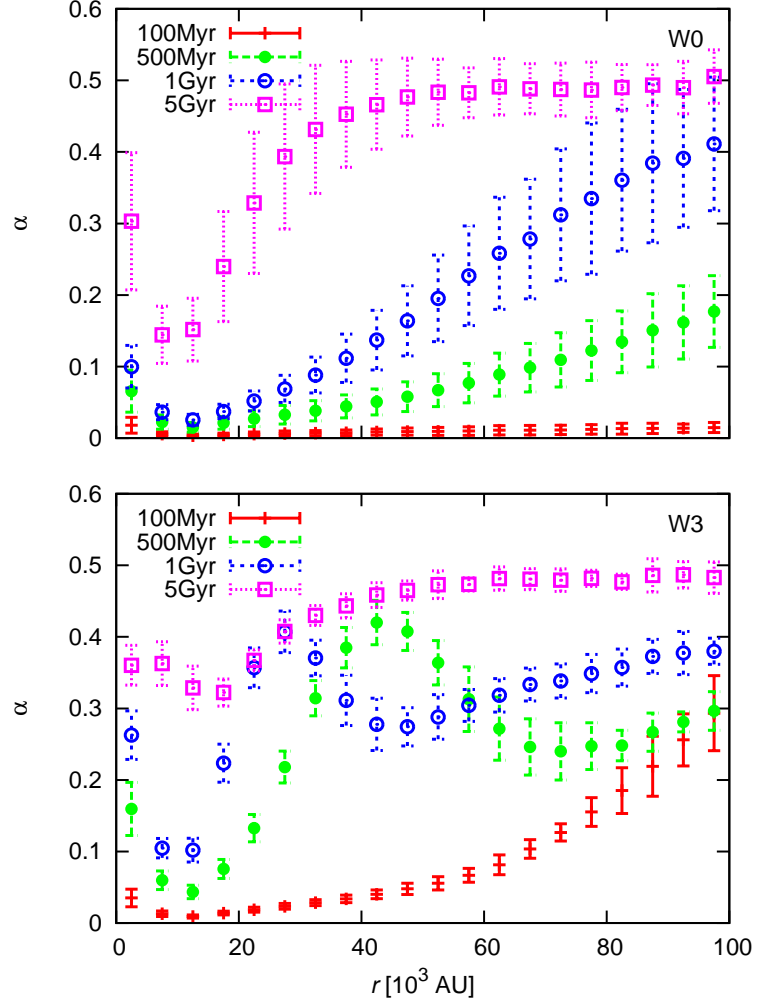


Fig. 14.— Normalized ratio of the vertical and radial axes α_r against r with $1\text{-}\sigma$ error bars for models W0 (top) and W4 (bottom) at $t=100$ Myr (crosses), 500 Myr (circles), 1 Gyr (open circles), and 5 Gyr (open squares).

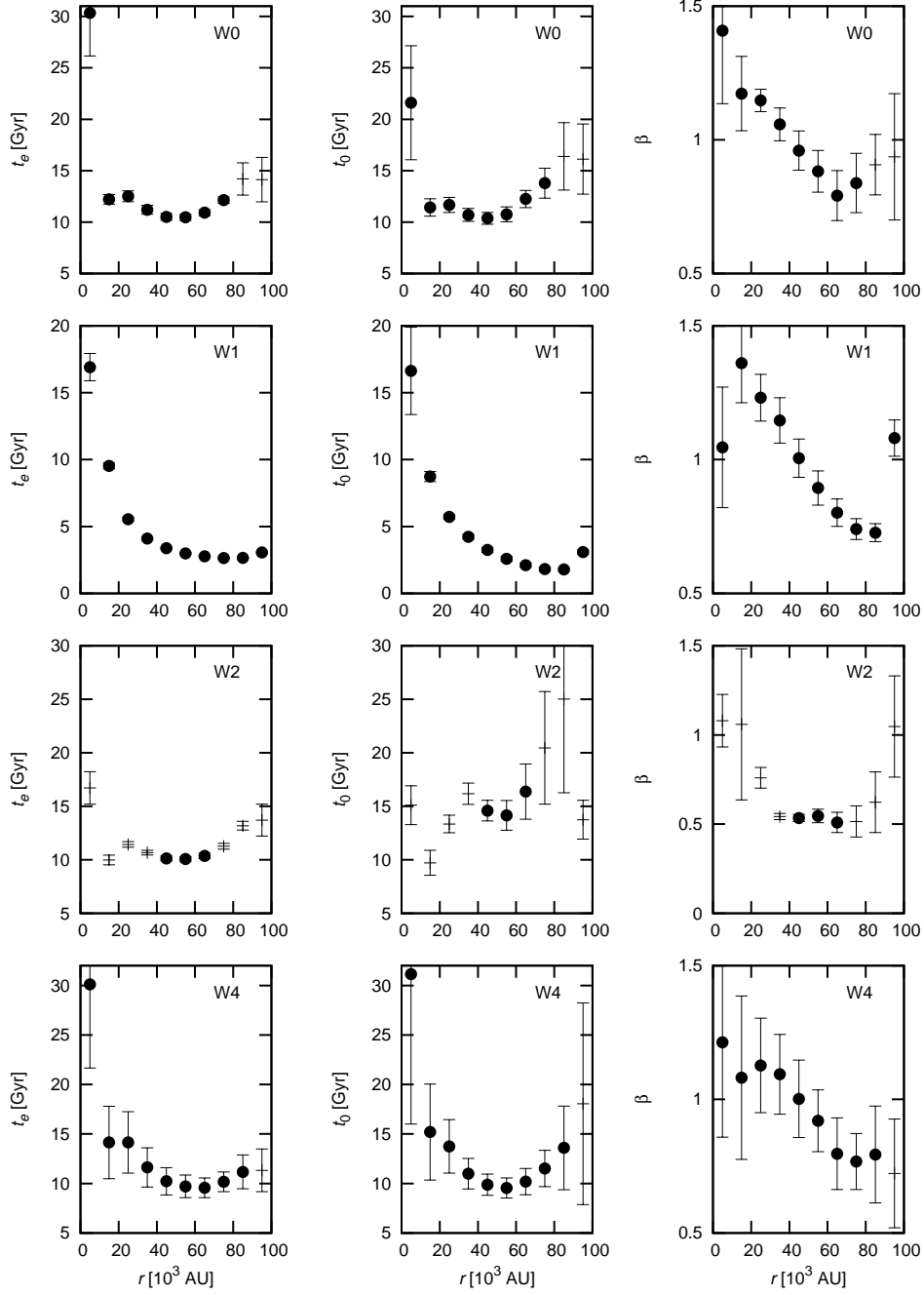


Fig. 15.— Standard e -folding time against r (left), the time t_0 for the Kohlrausch formula against r (middle), and the stretching parameter β for the Kohlrausch formula against r (right) for models W0, W1, W3, and W4 from the top. The data without filled circles are for the r -bins that do not have a monotonic decay.

Table 1: Model Parameters for Identical a_0 Disks

Model	a_0 [AU]	q_0 [AU]	i_0 [deg]	m_* [M_\odot]	f_{enc} [Myr^{-1}]	b_{max} [pc]	GT
I0	2×10^4	10	0	0.5	10	1	no
(variations)	5×10^3 - 5×10^4	10	0	0.25-2	2-20	1	no
I1	2×10^4	10	0	0.5	10	1	yes
I2	2×10^4	10 - 2×10^4	0-180	0.5	10	1	no
I3	2×10^4	10	0	Table 3		1	no
I4	2×10^4	10	0	0.5	10	0.25	no
I5	2×10^4	10	0	0.5	10	0.5	no
I6	2×10^4	10	0	0.5	10	2	no

Note. — For all, $n_0 = 10^4$, $v_* = 20 \text{ kms}^{-1}$, $b_{\text{min}} = 0.005 \text{ pc}$, and $b_{\text{max}} = 1 \text{ pc}$. The i_0 -distribution in I2 follows $dn/di_0 \propto \cos i_0$ (isotropic). GT means the additional Galactic tidal force.

Table 2: Model Parameters for Disks with a_0 -distribution

Model	γ	$m_* [M_\odot]$	$f_{\text{enc}} [\text{Myr}^{-1}]$	GT
W0	-2	0.5	10	no
W1	0	0.5	10	no
W2	1	0.5	10	no
W3	-2	0.5	10	yes
W4	-2	Table 3		no
W5	-3	0.5	10	no
W6	-1	0.5	10	no

Note. — For all, $n_0 = 5 \times 10^5$, $a_0 = 5 \times 10^3 - 5 \times 10^4 \text{AU}$, $q_0 = 10 \text{AU}$, $i_0 = 0$, $v_* = 20 \text{ kms}^{-1}$, $b_{\text{min}} = 0.005 \text{pc}$, and $b_{\text{max}} = 1 \text{pc}$. GT means the additional Galactic tidal force.

Table 3: Stellar parameters made from Table 1 in Rickman et al. (2008).

Stellar type	k	v_{\odot} [kms $^{-1}$]	σ [kms $^{-1}$]	f_{enc} [Myr $^{-1}$]	m_* [M_{\odot}]
B0	1	18.6	8.5	0.005	9
A0	2	17.1	11.4	0.03	3.2
A5	3	13.7	13.7	0.04	2.1
F0	4	17.1	16.8	0.15	1.7
F5	5	17.1	20.9	0.08	1.3
G0	6	26.4	21.6	0.22	1.1
G5	7	23.9	22.6	0.35	0.93
K0	8	19.8	19.7	0.34	0.78
K5	9	25.0	25.1	0.85	0.69
M0	10	17.3	24.7	1.29	0.47
M5	11	23.3	24.1	6.39	0.21
white dwarf	12	38.3	36.6	0.72	0.9
giant	13	21.0	23.7	0.06	4